1983

# High Speed Crack Propagation and Branching Under Uniaxial and Biaxial

S Anand
*University of Rhode Island*

# HIGH SPEED CRACK PROPAGATION AND BRANCHING UNDER UNIAXIAL AND BIAXIAL LOADING

BY

S. ANAND

A THESIS SUBMITTED IN PARTIAL FULFILLMENT OF THE REQUIREMENTS FOR THE DEGREE OF MASTER OF SCIENCE IN MECHANICAL ENGINEERING

UNIVERSITY OF RHODE ISLAND

1983

MASTER OF SCIENCE THESIS

OF

S. ANAND

APPROVED:

Thesis Committee

Major Professor Arun Shukla

M.H. Sadd

E.S. Mc Guire

R. Michel

DEAN OF THE GRADUATE SCHOOL

UNIVERSITY OF RHODE ISLAND

1983

ABSTRACT

A photoelastic investigation of high speed crack propagation and branching in a brittle polyester material called Homalite 100 was conducted for both uniaxial and biaxial loading conditions. Cross type specimens were loaded in a specially designed loading fixture where loads perpendicular and parallel to the crack could be controlled independently.

The photoelastic data obtained were analyzed to get the stress intensity factor K, the crack tip position a, the crack velocity $\dot{a}$ and other non-singular stress field coefficients including the stress acting parallel to the crack, $\sigma_{ox}$.

It was observed that K showed an increasing trend as the crack propagated through the specimens. Tensile stress parallel to the crack gave rise to higher stress intensity factors, compared to the compressive case for the same crack tip positions and initial normal loads. It was also found that tensile parallel remote stress enhanced branching and branching angle. While branching angles of 22° to 29° were encountered in uniaxial normal loading and biaxial tension-compression loading, angles as high as 45° and 73° were obtained in the tension-tension case.

It was concluded in this study that any crack branching criterion has to take into account the nature of the remote stress parallel to the crack and that crack branching is strongly influenced by non-singular stress field coefficients.

ACKNOWLEDGEMENTS

I would like to express my thanks and appreciation to my advisor, Dr. Shukla, for his guidance throughout this investigation. The help of the instrument shop in the project is also acknowledged. I would also like to add that this project was funded by the National Science Foundation under Grant No. MEA-8203277. The assistance of my colleague, K. Kumar, in carrying out the experiments, is also appreciated.

TABLE OF CONTENTS

## LIST OF FIGURES

List of Figures (cont'd)

List of Figures (cont'd)

## LIST OF TABLES

## LIST OF SYMBOLS

| | |
|---|---|
| $\dot{a}$ | crack velocity |
| $B_o'$ | normalized remote parallel stress |
| $c_1$ | dilatational wave velocity |
| $c_2$ | shear wave velocity |
| $c_R$ | Rayleigh wave velocity |
| $f_\sigma$ | material fringe value |
| G | shear modulus |
| $\lambda$ | modulus associated with dilatation |
| K | stress intensity factor |
| $K_{br}$ | branching stress intensity factor |
| $\rho$ | density of material |
| $\sigma_{ox}$ | remote parallel stress |
| $\sigma_x, \sigma_y$ $\tau_{xy}$ | stress components |
| $\tau_m$ | maximum in-plane shear stress |
| h | thickness of model |
| N | fringe order |
| N* | No. of data points |
| $\lvert\Delta n\rvert$ | average fringe order error |
| a* | crack tip position from edge of model |
| $A_0, A_1, A_2$ $B_0, B_1, B_2$ | series terms |

# 1. INTRODUCTION

This study is concerned with high speed crack propagation and branching in a brittle polyester model material called Homalite 100, under uniaxial and biaxial loading conditions.

High speed crack propagation and branching are of interest in several fields like mining and aircraft industries and large structures like nuclear reactors, pipelines, ships, etc. In the mining industry, one wants to optimize fragmentation and thus reduce the cost of mining operations by controlled fracturing. On the other hand, in structures like ships, bridges, pressure vessels etc., one wants to know if the crack will arrest after initiation or will go through the structure.

Dynamic fracture has always been one of the most important and difficult problems in mechanics. The existence of singularity at the crack tip and the inertia effects make it extremely difficult to obtain a solution by either analytical or numerical techniques. Researchers [1,2,3,4] have been attempting to characterize dynamic fracture in terms of a relation between the stress intensity factor, K and crack velocity $\dot{a}$ for different materials. However, till now, no study has been conducted to investigate the influence of non singular stress field coefficients on the $\dot{a}$-K behavior.

In the experimental studies of Fracture Mechanics, photoelasticity is a widely used technique to determine the stress intensity factor K at the crack tip. Though Post [5] and Wells and Post [6] applied photo-

elasticity to study the static and dynamic aspects of fracture and Irwin [7] developed a simple method to determine K from isochromatic fringe loops, the photoelastic community largely ignored fracture mechanics, in its formative period. Dixon [8] and Gerberich [9] were exceptions as they applied birefringent coatings to study strain fields near the crack tip in metallic plates.

In the past decade, major research programs in fracture mechanics have been started by C.W. Smith at Virginia Polytechnic Institute, A.S. Kobayashi at the University of Washington and J.W. Dally at the University of Maryland. C.W. Smith and his associates [10] have applied the stress-freezing technique to determine the stress intensity factor in a number of three dimensional crack problems. A.S. Kobayashi and his associates have used both dynamic photoelasticity and finite element methods to determine the dynamic state of stress at the tip of a propagating crack. Dally and his associates [2,11] have also employed dynamic photoelasticity in their studies of propagating cracks.

In photoelastic crack tip stress analysis, it is not advisable to use data from near the crack tip for practical reasons like fringe clarity, light scattering from the caustic at the crack tip, an unknown degree of plane strain constraint and so on [12]. In order to perform meaningful analysis from a larger and more desirable area in the stress field, additional non-singular terms have to be included. In this research, the equations derived by Irwin [13] were used and the series coefficients, including the stress intensity factor, were obtained using a multipoint over-deterministic technique developed by Sanford and Dally [14]. A total of six stress field coefficients were included for the analysis and a computer program was written in BASIC language

to obtain the values of the coefficients.

The results showed that the stress intensity factor, K and the far-field stress parallel to the crack, $\sigma_{ox}$, varied systematically as the crack propagated across the specimen and higher order terms showed an oscillatory behavior. The value of the stress intensity factor at branching seemed to vary slightly depending on the initial normal load applied. The branching angle depended on the nature of the far-field stress.

## 2. REVIEW OF RELATED RESEARCH ON HIGH SPEED CRACK PROPAGATION AND BRANCHING

Dynamic crack propagation and branching is best discussed in terms of crack propagation velocity $\dot{a}$ and the stress intensity factor, K. The Fracture Mechanics groups at the University of Maryland [1,2,3], University of Washington [4] and other institutions have made important contributions to the characterization of dynamic crack propagation by means of the relationship between the crack velocity and the stress intensity factor.

Irwin, Dally and others [1] performed a series of fracture tests with various types of specimens fabricated from Homalite 100 and observed that the $\dot{a}$ versus K curve had three distinct regions, the stem, the slope range and the plateau, as shown in Fig. 1. In the stem region, the crack velocity is independent of K. Small changes of K cause considerable changes in the crack velocity, up to velocities of about 200 m/s. The slope range is the transition region covering crack velocities from 200 to 381 m/s. For higher velocities, a large increase in K is needed even for small increases in $\dot{a}$. This is the plateau region. The highest velocity of crack propagation recorded in these experiments was 432 m/s. Rossmanith and Irwin [3] suggested that the $\dot{a}$ vs K relationship, as obtained from experiments with test specimens, depends in the high velocity region on the type of test specimen used. Irwin et al [1] concluded that the value $K_{Im}$, which is the stress intensity factor below which the crack cannot propagate, can be treated

as a material property. Though it has been shown theoretically [16] that the maximum crack velocity which can be achieved is $\dot{a} = c_R$, the Rayleigh wave velocity, this value is not attained for most of the materials in practice because branching occurs at lower velocities and the energy driving the crack is divided. Dally and his associates [2] observed that in the case of Homalite 100, branching occurs with the SEN specimen when $\dot{a}/c_2 = 0.32$ to 0.35. The velocity at branching is often called the terminal velocity $\dot{a}_T$ and it is generally believed that $\dot{a}_T$ is the maximum which can be achieved for a given material. However super-velocities of the order of 726 m/s were obtained by explosive testing wherein branching was suppressed to an extent by stress waves [2].

Coming to the phenomenon of crack branching, numerous researchers have performed prebranching and post branching analyses but their results rarely agree. Pre branching analysis looks for criteria for crack branching while post branching analysis deals primarily with the direction and the propagation of the branched crack.

Yoffe [16] was the first to study the dynamic stress field around a moving crack tip and found that the circumferential stress $\sigma_{\theta\theta}$ reaches a maximum at an angle of 60° for $\dot{a}/c_2 = 0.6$ which is different from its original direction of $\theta = 0$ for lower crack velocities. It was also concluded that the branching angle was 2x60° = 120°. Craggs [17] derived a critical crack velocity of $\dot{a}/c_1 = 0.4$ for a propagating semi-infinite crack. However, in experiments, velocities close to the critical velocity were never attained and in phenomena like stress corrosion cracking, branching occurred at very low velocities. So some other parameter, rather than just the velocity, should be connected with branching. Clark and Irwin [18] suggested that the dynamic stress

intensity factor should reach a critical value, $K_b$ (or the strain energy release rate should reach a critical value, $G_b$) for branching to occur at terminal velocity. Kalthoff [19] found that there is a characteristic forking angle in which case the branches neither repel nor attract each other. The corresponding branching angle was about 30°.

Kobayashi et al [4] observed that the branching stress intensity factor for Homalite 100 was approximately three times the fracture toughness. K values of the order of 1.54 and 1.98 MPa$\sqrt{m}$ were encountered for 3/8" and 1/8" thick sheets at branching. These values were equal to the maximum K observed in fractured plates without branches. The results indicated that the dynamic stress intensity factor was a necessary but not sufficient condition for branching. The combination of excessively large strain energy release rate, shown by the large static stress intensity factor, available at the time when the running crack tip is subjected to a maximum dynamic stress intensity factor, could be a plausible cause for the crack to branch.

Dally et al [2] obtained crack branching at branching stress intensity factor, $K_{Ib}$ ranging from 3.3 to 3.8 times $K_{Im}$, the arrest toughness when the crack moved at terminal velocity in Homalite 100. Research by Dally, Kobayashi and others pointed to the fact that $K_{Ib}$ is not a material property, contrary to results obtained by Congleton, Anthony [20,21] and Doll [22]. Kirchner [23] found that $K_{Ib}$ and Young's Modulus had a strong correlation and developed a strain intensity criterion for crack branching in ceramics. Ramulu et al [15] have developed a branching criterion which contends that a necessary and sufficient condition for branching is a crack branching stress intensity factor, $K_{Ib}$, accompanied by a minimum characteristic distance

$r_o = r_c$. H.P. Rossmanith and G.R. Irwin [3] suggested that non-singular stress field coefficients may influence $\dot{a}$-K behavior in the terminal velocity region. Till now, no research has been conducted on high velocity crack propagation and branching by systematically varying the non-singular coefficients. This is the objective of this project.

## 3. THE MULTIPLE SPARK CAMERA AND ITS APPLICATION TO DYNAMIC PHOTOELASTICITY

Crack propagation studies need a high speed recording system to take pictures of the transient crack tip stress patterns in dynamic photoelastic stress analysis. One of the most frequently used recording systems is the Multiple Spark Camera, originally designed by Cranz and Schardin [25]. A camera similar to this was designed and built at URI and is housed in the Photomechanics Laboratory. This chapter will briefly discuss the method of photoelasticity and the components of the Spark gap Camera.

Many transparent noncrystalline materials that are optically isotropic when free of stress become optically anisotropic and display characteristics similar to crystals when they are stressed. These characteristics persist while loads on the material are maintained but disappear when the loads are removed. This behavior is called temporary double refraction and the method of photoelasticity is based on this physical behavior of transparent noncrystalline materials [26].

For experimentation, the model is fabricated from a polymeric, transparent, birefringent material. When circularly polarized light passes through the stressed model and then through another circular polarizer, an optical interference occurs due to stress-induced birefringence in the model. This optical interference produces a series of light and dark bands which are termed isochromatic fringe patterns. The stress optic law, which relates the stress state of the model to

the order of the associated interference pattern is given by

$2\tau_m = \sigma_1 - \sigma_2 = Nf_\sigma/h$,

where $\sigma_1$ and $\sigma_2$ are the in-plane principal stresses, $\tau_m$ the maximum in-plane shear stress, N the fringe order, $f_\sigma$ the material fringe value and h the thickness of the model. In dynamic photoelasticity, the fringes move at high velocities and so a high speed recording system like the Multiple Spark Camera is used for purposes of stress analysis.

## 3.1 Description of the Camera

The camera consists of three main subdivisions, viz., the spark gap circuit, the optical arrangement and the control circuit.

3.1.1 The Spark Circuit - The Multiple Mach spark circuit is shown in Fig. 2. In the camera that was used in this project, there are twenty spark gaps (SG), each of them connected to L-C circuits in series. TSG is the trigger spark gap. In operation the condensers are charged to about 15 KV and the circuit $L_1C_1$ closed by applying a trigger pulse to the spark gap TSG. The firing sequence is initiated at a predetermined time after the crack initiation by applying a 30 KV pulse to the trigger gap. When the trigger gap is fired, the capacitor $C_1$ discharges to below the ground potential. When the voltage on $C_1$ becomes sufficiently negative, a spark occurs at gap $SG_1$ and capacitor $C_1^*$ discharges, producing a short, intense flash of light.

The timing between the first and second sparks depends on the inductance $L_2$ in the $C_1^* L_2C_2$ loop. When the gap SG1 fires, the voltage on $C_2$ decays with time and the gap SG2 fires when the voltage on $C_2$ is sufficiently negative. Likewise, all the twenty gaps fire. The light from the spark gaps is led out of the camera by fibre optics.

Optical Arrangement - The optical setup is shown in Fig. 3. Two circular polarizers are kept on each side of the specimen. As an example, light from the spark SG1 passes through a field lens, the first polarizer, the specimen, the second polarizer and the second field lens onto the camera lens $L_1$. In a similar manner, light from spark Gaps SG2, SG3, SG4 etc. is focused on the corresponding camera lenses $L_2$, $L_3$, $L_4$ etc. The spark gaps, the field lenses and the camera lenses are so placed that the light from one particular spark falls on one particular camera lens so that the image from one camera lens is due to one spark only. So twenty pictures of the propagating crack are obtained at twenty different spots on the same film. Kodak Wratten No. 8 filters and Kodak Grauvre Positive 4135 film are used, the combination of film and filter yielding blue light of wavelength of 4920Å.

3.1.3 Control Circuit - The control circuit is used to initiate the firing sequence at a required delay after the dynamic event is started. A schematic ofthe circuit is shown in Fig. 4 [27]. When the conductive paint on the specimen is broken by the moving crack, a 20V pulse is emitted which initiates a Digital Delay Generator (Model 103CR of California Avionics Labs Inc.) and a Nicolet Oscilloscope (Model 206).

The light from the sparks is picked up by a high frequency response photocell and its output is recorded on the oscilloscope as an Intensity Time trace. The timings of the peaks on this trace represent the time at which the picture of the crack was taken. The delay generator holds the pulse from the broken conductive paint line for a predetermined interval of time. Once the pulse is passed to the Trigger Spark Gap after the required delay, the voltage at the trigger gap is stepped

up to about 30 KV, after which the firing occurs in the sequence as described before.

## 4. CRACK TIP STRESS FIELD ANALYSIS

### Derivation of the Dynamic Equations

The analysis shall make use of Irwin's crack tip stress function [28] and shall assume plane strain ($\varepsilon_z = 0$). The leading edge of the crack will be taken as the positive x-axis and the crack tip as the origin of the coordinate system, as shown in Fig. 5.

For crack propagation in the x-direction and assuming that the stress field does not change with time with respect to the moving coordinate system, the following equations apply:

$$\frac{\partial^2 u}{\partial t^2} = c^2 \frac{\partial^2 u}{\partial x^2} \tag{4.1}$$

$$\frac{\partial^2 v}{\partial t^2} = c^2 \frac{\partial^2 v}{\partial x^2} \tag{4.2}$$

where u and v are the displacements in the x and y directions and c the crack velocity.

Equilibrium conditions in the x and y directions lead to the following results:

$$\frac{\partial \sigma_x}{\partial x} + \frac{\partial \tau_{xy}}{\partial y} = \rho \frac{\partial^2 u}{\partial t^2} = \rho c^2 \frac{\partial^2 u}{\partial x^2} \tag{4.3}$$

$$\frac{\partial \tau_{xy}}{\partial x} + \frac{\partial \sigma_y}{\partial y} = \rho \frac{\partial^2 v}{\partial t^2} = \rho c^2 \frac{\partial^2 v}{\partial x^2} \tag{4.4}$$

where $\sigma_x$, $\sigma_y$ and $\tau_{xy}$ are the stress components and $\rho$ the density of the body.

Using Hooke's law in the form

$$\sigma_x = \lambda\Delta + 2G\varepsilon_x \tag{4.5}$$

$$\sigma_y = \lambda\Delta + 2G\varepsilon_y \tag{4.6}$$

$$\sigma_{xy} = G\gamma_{xy} \tag{4.7}$$

where G is the shear modulus and $\lambda$ the modulus associated with dilatation.

We can rewrite the equations (4.3) and (4.4) in terms of dilatation $\Delta$ and rotation $\omega$, where

$$\Delta = \frac{\partial u}{\partial x} + \frac{\partial v}{\partial y} \tag{4.8}$$

$$\omega = \frac{\partial v}{\partial x} - \frac{\partial u}{\partial y} \tag{4.9}$$

Equations (4.3) and (4.4) then take the following form,

$$(\lambda+2G)\ \frac{\partial \Delta}{\partial x} - G\ \frac{\partial \omega}{\partial y} = \rho c^2\ \frac{\partial^2 u}{\partial x^2} \tag{4.10}$$

$$G\ \frac{\partial \omega}{\partial x} + (\lambda+2G)\ \frac{\partial \Delta}{\partial y} = \rho c^2\ \frac{\partial^2 v}{\partial x^2} \tag{4.11}$$

Noting that

$$\frac{\partial}{\partial x}\left(\frac{\partial^2 u}{\partial x^2}\right) + \frac{\partial}{\partial y}\left(\frac{\partial^2 v}{\partial x^2}\right) = \frac{\partial^2 \Delta}{\partial x^2} \tag{4.12}$$

and $$\frac{\partial}{\partial x}\left(\frac{\partial^2 v}{\partial x^2}\right) - \frac{\partial}{\partial y}\left(\frac{\partial^2 u}{\partial x^2}\right) = \frac{\partial^2 \omega}{\partial x^2} \tag{4.13}$$

we can derive the equations

$$(\lambda+2G)\nabla^2(\Delta) = \rho c^2\ \frac{\partial^2 \Delta}{\partial x^2} \tag{4.14}$$

$$G\nabla^2\omega = \rho c^2 \frac{\partial^2 \omega}{\partial x^2} \tag{4.15}$$

Equations (4.14) and (4.15) can be simplified in appearance in the following ways. In equation (4.14), we substitute $y_1 = \lambda_1 y$ where

$$\lambda_1^2 = 1 - (\frac{c}{c_1})^2 = 1 - \frac{\rho c^2}{\lambda+2G} \tag{4.16}$$

In equation (4.15), we substitute $y_2 = \lambda_2 y$, where

$$\lambda_2^2 = 1 - (\frac{c}{c_2})^2 = 1 - \frac{\rho c^2}{G} \tag{4.17}$$

The resulting pair of equations is

$$\frac{\partial^2 \Delta}{\partial x^2} + \frac{\partial^2 \Delta}{\partial y_1^2} = 0 \tag{4.18}$$

$$\frac{\partial^2 \omega}{\partial x^2} + \frac{\partial^2 \omega}{\partial y_2^2} = 0 \tag{4.19}$$

Clearly $\Delta$ is a harmonic function of x and $\lambda_1 y$ while $\omega$ is a harmonic function of x and $\lambda_2 y$.

It can be shown there is no loss of generality for the proposed problem [13] if we assume

$$\Delta = (1-\lambda_1^2)A \text{ Re } Z_1 \tag{4.20}$$

$$\omega = (1-\lambda_2^2)B \text{ Im } Z_2 \tag{4.21}$$

where $Z_1 = f'(z_1)$, $Z_2 = f'(z_2)$, $z_1 = x+iy_1$ and $z_2 = x+iy_2$.

In addition it is helpful to recognize that the displacements can be divided into non rotational $(u_1, v_1)$ and nondilatational $(u_2, v_2)$ components. Thus $u = u_1+u_2$, $v = v_1+v_2$ where

$$\Delta = \frac{\partial u_1}{\partial x} + \lambda_1 \frac{\partial v_1}{\partial y_1} = (1-\lambda_1^2)A \text{ Re } Z_1 \tag{4.22}$$

$$\frac{\partial v_1}{\partial x} - \lambda_1 \frac{\partial u_1}{\partial y_1} = 0 \tag{4.23}$$

Also

$$\omega = \frac{\partial v_2}{\partial x} - \lambda_2 \frac{\partial u_2}{\partial y_2} = (1-\lambda_2^2)B \text{ Im } Z_2 \tag{4.24}$$

$$\frac{\partial u_2}{\partial x} + \lambda_2 \frac{\partial v_2}{\partial y_2} = 0 \tag{4.25}$$

Comparing equations 4.22 and 4.23, we get

$$\left.\begin{aligned} u_1 &= A \text{ Re } [f(z_1)] \\ v_1 &= -\lambda_1 A \text{ Im } [f(z_1)] \end{aligned}\right\} \tag{4.26}$$

Similarly from equations 4.24 and 4.25,

$$\left.\begin{aligned} u_2 &= -\lambda_2 B \text{ Re } [f(z_2)] \\ v_2 &= B \text{ Im } [f(z_2)] \end{aligned}\right\} \tag{4.27}$$

Since the shear stress on the crack faces is zero, $\tau_{xy} = 0$ on $y = 0$ for $x < 0$. Along this line $f'(z_1) = f'(z_2) = f'(x)$. One finds that on $y = 0$

$$\frac{1}{G}\tau_{xy} = \gamma_{xy} = [-2\lambda_1 A + (1+\lambda_2^2)B]\text{Im}[f'(x)] \tag{4.28}$$

Since $\text{Im}[f'(x)]$ on $y = 0$ is not zero along the entire x axis, we must assume

$$B = \frac{2\lambda_1}{1+\lambda_2^2} \cdot A \tag{4.29}$$

In order to determine A, consider next that

$$f'(z) = \sum_{n=0} A_n z^{n-\frac{1}{2}} \tag{4.30}$$

Since $\frac{\partial u}{\partial x}$ and $\frac{\partial v}{\partial y}$ are proportional to Re[f'(x)] along y = 0, equation (4.30) ensures $\sigma_x$ and $\sigma_y = 0$ when x is negative. When x is positive, $\sigma_y$ is not zero.

'A' can be determined from the defining equation for the Stress Intensity Factor, K. That is, for x very small and positive and y = 0

$$\sigma_y = \frac{K}{\sqrt{2\pi x}} = \lambda\Delta + 2G \frac{\partial v}{\partial y} \tag{4.31}$$

From previous expressions

$$\lambda\Delta = \lambda(1-\lambda_1^2)A\, A_o/\sqrt{x}$$

$$2G \frac{\partial v_1}{\partial y} = 2G\, \lambda_1 \frac{\partial v_1}{\partial y_1} = -2G\lambda_1^2 A\, A_o/\sqrt{x}$$

$$2G \frac{\partial v_2}{\partial y} = 2G\lambda_2 \frac{\partial v_2}{\partial y_2} = 2G \frac{2\lambda_1\lambda_2}{1+\lambda_2^2} A \cdot A_o/\sqrt{x}$$

When the above relations are inserted into equation 4.30, it is convenient to replace $\lambda$ using the equation

$$(\lambda+2G) = \frac{(1-\lambda_2^2)}{(1-\lambda_1^2)} G \tag{4.32}$$

It is also convenient to assume $K = A_o\sqrt{2\pi}$. This can be done because all of the constant coefficients in equation (4.30) must be adjusted to fit the boundary conditions.

$$\text{Thus} \quad A = \frac{1}{G} \frac{1}{\left[\frac{4\lambda_1\lambda_2}{1+\lambda_2^2} - (1+\lambda_2^2)\right]} \tag{4.33}$$

The expressions for $\sigma_x$, $\sigma_y$ and $\tau_{xy}$ are derived as follows:

$$\sigma_x = \lambda\Delta + 2G\frac{\partial u}{\partial x}$$

$$= \lambda(1-\lambda_1^2)A \text{ Re } Z_1$$

$$+ 2G(A \text{ Re } Z_1 - \lambda_2 B \text{ Re } Z_2) \qquad (4.34)$$

We know from eqn. (4.29) that

$$B = \frac{2\lambda_1}{1+\lambda_2^2} A$$

and from eqn. (4.32) that

$$\lambda = G\left[\frac{1-\lambda_2^2}{1-\lambda_1^2} - 2\right]$$

Substituting these in eqn. (4.34)

$$\sigma_x = G(2\lambda_1^2-\lambda_2^2-1)A \text{ Re } Z_1$$

$$+ 2G\left[A \text{ Re } Z_1 - \lambda_2 \frac{4\lambda_1}{1+\lambda_2^2} A \text{ Re } Z_2\right]$$

$$= AG\left[(1+2\lambda_1^2 - \lambda_2^2)\text{Re } Z_1 - \frac{4\lambda_1\lambda_2}{1+\lambda_2^2} \text{Re } Z_2\right] \qquad (4.35)$$

Similarly we can obtain

$$\sigma_y = AG\left[-(1+\lambda_2^2)\text{Re}Z_1 + \frac{4\lambda_1\lambda_2}{1+\lambda_2^2} \text{Re } Z_2\right] \qquad (4.36)$$

and $$\tau_{xy} = AG \cdot 2\lambda_1[\text{Im } Z_2 - \text{Im } Z_1] \qquad (4.37)$$

where $AG = \dfrac{1}{\left[\dfrac{4\lambda_1\lambda_2}{1+\lambda_2^2} - (1+\lambda_2^2)\right]}$ from eqn. (4.33)

and $\dfrac{1-\lambda_1^2}{1-\lambda_2^2} = c_2^2/c_1^2$

A second choice for the function Z can be made in the form

$$Y = \sum_{m=0} B_m z^m \tag{4.38}$$

One can observe that on $y = 0$ and for any value of x, $Y_1$ and $Y_2$ have zero imaginary parts. Thus $\tau_{xy} = 0$ on $y = 0$. In order to have $\sigma_y = 0$ on the line segment occupied by the crack, it is necessary to require

$$B = \frac{1+\lambda_2^2}{2\lambda_2} \cdot A \tag{4.39}$$

The resulting stress equations are

$$\sigma_x = AG[(1+2\lambda_1^2-\lambda_2^2)ReY_1 - (1+\lambda_2^2)ReY_2] \tag{4.40}$$

$$\sigma_y = AG(1+\lambda_2^2)(ReY_2-ReY_1) \tag{4.41}$$

$$\tau_{xy} = AG[(1+\lambda_2^2)^2 \frac{ImY_2}{2\lambda_2} - 2\lambda_1 ImY_1] \tag{4.42}$$

AG in equations (4.40)-(4.42) can be obtained by using the boundary condition $\sigma_x = \sigma_{ox} = 2B_o$ as $x \to 0$ on the positive x-axis. So from equation (4.40), we get $\sigma_x$ as $x \to 0 = AG[(1+2\lambda_1^2-\lambda_2^2)ReY_1-(1+\lambda_2^2)ReY_2]$ where $ReY_1 = ReY_2 = B_o$ from equation (4.38) i.e. $\sigma_{ox} = 2AG[\lambda_1^2-\lambda_2^2]B_o$. Assuming that $\sigma_x$ as r and $\theta \to 0$ is a constant value of $\sigma_{ox} = 2B_o$, we get

$$AG = \frac{1}{[\lambda_1^2-\lambda_2^2]}$$

Since the above two series functions satisfy the boundary conditions of the problem, the sum of the two should also satisfy the boundary conditions.

$$\text{So } \sigma_x = \frac{1}{[\Omega-(1+\lambda_2^2)]} \cdot [(1+2\lambda_1^2-\lambda_2^2)\mathrm{Re}Z_1 - \Omega\mathrm{Re}Z_2]$$

$$+ \frac{1}{(\lambda_1^2-\lambda_2^2)} [(1+2\lambda_1^2-\lambda_2^2)\mathrm{Re}Y_1 - (1+\lambda_2^2)\mathrm{Re}Y_2] \tag{4.43}$$

$$\sigma_y = \frac{1}{[\Omega-(1+\lambda_2^2)]} [-(1+\lambda_2^2)\mathrm{Re}Z_1 + \Omega\mathrm{Re}Z_2]$$

$$+ \frac{(1+\lambda_2^2)}{(\lambda_1^2-\lambda_2^2)} (\mathrm{Re}Y_2 - \mathrm{Re}Y_1) \tag{4.44}$$

$$\tau_{xy} = \frac{1}{[\Omega-(1+\lambda_2^2)]} \cdot 2\lambda_1(\mathrm{Im}Z_2-\mathrm{Im}Z_1)$$

$$+ \frac{1}{(\lambda_1^2-\lambda_2^2)} \left[\frac{(1+\lambda_2^2)^2}{2\lambda_2} \mathrm{Im}Y_2 - 2\lambda_1\mathrm{Im}Y_1\right] \tag{4.45}$$

where $\Omega = 4\lambda_1\lambda_2/(1+\lambda_2^2)$

From equations (4.43) and (4.44), we obtain

$$\frac{\sigma_y-\sigma_x}{2} = \frac{1}{[\Omega-(1+\lambda_2^2)]} [\Omega\mathrm{Re}Z_2-(1+\lambda_1^2)\mathrm{Re}Z_1]$$

$$+ \frac{1}{(\lambda_1^2-\lambda_2^2)} [(1+\lambda_2^2)\mathrm{Re}Y_2-(1+\lambda_1^2)\mathrm{Re}Y_1] \tag{4.46}$$

The first three terms in each of the series Z and Y shall be included in the analysis. So $Z_1$ and $Z_2$ can be expressed as follows:

$$Z_1 = A_o z_1^{-\frac{1}{2}} + A_1 z_1^{\frac{1}{2}} + A_2 z_1^{\frac{3}{2}} \text{ and} \tag{4.47}$$

$$Z_2 = A_o z_2^{-\frac{1}{2}} + A_1 z_2^{\frac{1}{2}} + A_2 z_2^{\frac{3}{2}} \tag{4.48}$$

$Y_1$ and $Y_2$ can be expressed as

$$Y_1 = B_o + B_1 z_1 + B_2 z_1^2 \tag{4.49}$$

$$Y_2 = B_o + B_1 z_2 + B_2 z_2^2 \tag{4.50}$$

where $A_o\sqrt{2\pi} = K$, the stress intensity factor and remote stress $\sigma_{ox} = 2B_o$.

$$z_1 = \rho_1 e^{i\phi_1} \quad \text{and} \quad z_2 = \rho_2 e^{i\phi_2} \tag{4.51}$$

where $\rho_1$, $\rho_2$, $\phi_1$ and $\phi_2$ are shown in Fig. (6). Substituting for $z_1$ and $z_2$ in equations (4.47) to (4.50) and separating the real and imaginary parts, we get

$$\mathrm{Re}Z_1 = A_o\rho_1^{-\frac{1}{2}}\cos\frac{\phi_1}{2} + A_1\sqrt{\rho_1}\cos\frac{\phi_1}{2} + A_2\rho_1^{\frac{3}{2}}\cos\left(\frac{3\phi_1}{2}\right) \tag{4.52}$$

$$\mathrm{Im}Z_1 = -A_o\rho_1^{-\frac{1}{2}}\sin\frac{\phi_1}{2} + A_1\sqrt{\rho_1}\sin\frac{\phi_1}{2} + A_2\rho_1^{\frac{3}{2}}\sin\frac{3\phi_1}{2} \tag{4.53}$$

Replacing $z_1$ by $z_2$ in equations (4.52) and (4.53)

$$\mathrm{Re}Z_2 = A_o\rho_2^{-\frac{1}{2}}\cos\left(\frac{\phi_2}{2}\right) + A_1\sqrt{\rho_2}\cos\frac{\phi_2}{2} + A_2\rho_2^{\frac{3}{2}}\cos\left(\frac{3\phi_2}{2}\right) \tag{4.54}$$

and

$$\mathrm{Im}Z_2 = -A_o\rho_2^{-\frac{1}{2}}\sin\frac{\phi_2}{2} + A_1\sqrt{\rho_2}\sin\frac{\phi_2}{2} + A_2\rho_2^{\frac{3}{2}}\sin\left(\frac{3\phi_2}{2}\right) \tag{4.55}$$

Similarly,

$$\mathrm{Re}Y_1 = B_o + B_1\rho_1\cos\phi_1 + B_2\rho_1^2\cos 2\phi_1 \tag{4.56}$$

$$\mathrm{Im}Y_1 = B_1\rho_1\sin\phi_1 + B_2\rho_1^2\sin 2\phi_1 \tag{4.57}$$

$$\mathrm{Re}Y_2 = B_o + B_1\rho_2\cos\phi_2 + B_2\rho_2^2\cos 2\phi_2 \tag{4.58}$$

$$\mathrm{Im}Y_2 = B_1\rho_2\sin\phi_2 + B_2\rho_2^2\sin 2\phi_2 \tag{4.59}$$

From Fig. 6, it is evident that

$$\phi_1 = \text{Tan}^{-1}[\lambda_1 \tan\theta] \tag{4.60}$$

and

$$\phi_2 = \text{Tan}^{-1}[\lambda_2 \tan\theta] \tag{4.61}$$

$$\rho_1 = r[1-(1-\lambda_1^2)\sin^2\theta]^{\frac{1}{2}} \tag{4.62}$$

$$\rho_2 = r[1-(1-\lambda_2^2)\sin^2\theta]^{\frac{1}{2}} \tag{4.63}$$

where $\lambda_1 = [1-(\frac{c}{c_1})^2]^{\frac{1}{2}}$ and $\lambda_2 = [1-(\frac{c}{c_2})^2]^{\frac{1}{2}}$

Substituting the expressions (4.52) to (4.59) in equations (4.45) and (4.46) and making use of eqns. (4.60) to (4.63), we can obtain expressions for $\frac{\sigma_y-\sigma_x}{2}$ and $\tau_{xy}$ in terms of the series constants and the polar coordinates r and $\theta$.

## 2 Application of Photoelasticity to the Dynamic Equations:

The stress optic law, which relates the optical properties of the material to its stress state, is given by

$$2\tau_m = Nf_\sigma/h \tag{4.64}$$

where $\tau_m$ is the maximum in plane shear stress, $f_\sigma$ the material fringe value, h the thickness of the model and N the order of the fringe in consideration.

It is known that

$$(2\tau_m)^2 = (\sigma_y-\sigma_x)^2 + 4\tau_{xy}^2.$$

i.e. $$\tau_m^2 = \left(\frac{\sigma_y-\sigma_x}{2}\right)^2 + \tau_{xy}^2 \qquad (4.65)$$

Combining eqns. (4.64) and (4.65), we get

$$(Nf_\sigma/2h)^2 = \left(\frac{\sigma_y-\sigma_x}{2}\right)^2 + \tau_{xy}^2 \qquad (4.66)$$

The expressions for $\frac{\sigma_y-\sigma_x}{2}$ and $\tau_{xy}$ (4.46) and (4.45) can be substituted into eqn. (4.66) to obtain an equation connecting the series constants, the fringe order, the material fringe value and the polar coordinates r and $\theta$. The function $\left(\frac{Nf_\sigma}{2h}\right)^2 - \left(\frac{\sigma_y-\sigma_x}{2}\right)^2 - \tau_{xy}^2$ is denoted by $G_K$ and $\frac{\sigma_y-\sigma_x}{2}$ and $\tau_{xy}$ are denoted by D and T respectively.

i.e. $$G_K = (Nf_\sigma/2h)^2 - D^2 - T^2 \text{ , at the } K^{th} \text{ data point.} \qquad (4.67)$$

A combination of least squares and Newton-Raphson techniques is applied to this function as follows.

## 4.3 The Overdeterministic Method:

The approach used is that suggested by Sanford and Dally [14]. The series constants have to be determined to make $G_K = 0$. Though equation (4.67) can be solved in closed form, the algebra becomes quite involved and a simpler numerical method based on the Newton-Raphson technique is employed.

In the overdeterministic method, the function $G_K$ is evaluated at a large number of data points in the stress field. If initial estimates are given for the series constants in eqn. (4.67), $G_K \neq 0$, since the initial estimates will usually be in error. To correct the estimates, a series of iterative equations based on a Taylor series expansion of $G_K$ are written as

$$(G_K)_{i+1} = (G_K)_i + [\frac{\partial G_K}{\partial A_o}]\Delta A_o + [\frac{\partial G_K}{\partial A_1}]\Delta A_1 + \ldots. \tag{4.68}$$

where the subscript i refers to the $i^{th}$ iteration step and $\Delta A_o$, $\Delta A_1$, etc. are corrections for the previous estimates of $A_o$, $A_1$ etc.

The corrections are determined so that $(G_K)_{i+1} = 0$ and thus eqn. (4.68) gives

$$[\frac{\partial G_K}{\partial A_o}]\Delta A_o + [\frac{\partial G_K}{\partial A_1}]\Delta A_1 + \ldots. = - (G_K)_i \tag{4.69}$$

The method of least squares involves the determination of the series coefficients so that eqn. (4.67) is fitted to a large number of data points in the isochromatic field.

Eqn. (4.69) in the matrix form gives

$$\begin{bmatrix} G_1 \\ G_2 \\ \cdot \\ \cdot \\ G_N \end{bmatrix} = \begin{bmatrix} \Delta A_o \\ \Delta A_1 \\ \Delta A_2 \\ \Delta B_o \\ \Delta B_1 \\ \Delta B_2 \end{bmatrix} \quad X \quad \begin{bmatrix} \frac{\partial G_1}{\partial A_o} & \frac{\partial G_1}{\partial A_1} & \cdots & \frac{\partial G_1}{\partial B_2} \\ \frac{\partial G_2}{\partial A_o} & \frac{\partial G_2}{\partial A_1} & \cdots & \frac{\partial G_2}{\partial B_2} \\ \cdot & \cdot & \cdots & \cdot \\ \cdot & \cdot & \cdots & \cdot \\ \frac{\partial G_N}{\partial A_o} & \frac{\partial G_N}{\partial A_1} & \cdots & \frac{\partial G_n}{\partial B_2} \end{bmatrix}$$

where N is the total number of data points considered. The above equation can be put in the form

$$G = [a][\Delta A] \tag{4.70}$$

where $G = \begin{bmatrix} G_1 \\ G_2 \\ \vdots \\ G_N \end{bmatrix}$ $\Delta A = \begin{bmatrix} \Delta A_o \\ \Delta A_1 \\ \vdots \\ \Delta B_2 \end{bmatrix}$

and $[a] = -\begin{bmatrix} \frac{\partial G_1}{\partial A_o} & \frac{\partial G_1}{\partial A_1} & \cdots & \frac{\partial G_1}{\partial B_2} \\ \frac{\partial G_2}{\partial A_o} & \frac{\partial G_2}{\partial A_1} & \cdots & \frac{\partial G_2}{\partial B_2} \\ \vdots & \vdots & & \vdots \\ \frac{\partial G_N}{\partial A_o} & \frac{\partial G_N}{\partial A_1} & \cdots & \frac{\partial G_N}{\partial B_2} \end{bmatrix}$

Premultiplying by $a^T$ (Transpose of a),

$$[a]^T G = [a]^T [a][\Delta A] \text{ or}$$

$$[d] = [c][\Delta A] \quad \text{where} \quad [d] = [a]^T G$$

and $[c] = [a]^T [a]$

The correction factors are given by

$$[\Delta A] = [c]^{-1}[d] \tag{4.71}$$

The iterative procedure is employed till the series constants are determined to obtain a close fit of the function G to the N data points.

The differentials of G with respect to the series coefficients are obtained as follows:

Differentiating eqn. (4.67) with respect to $A_o$ gives

$$\frac{\partial G_K}{\partial A_o} = 2D \frac{\partial D}{\partial A_o} + 2T \frac{\partial T}{\partial A_o} \tag{4.72}$$

$$\frac{\partial D}{\partial A_o} = \frac{\partial}{\partial A_o}\left[\frac{\sigma_y - \sigma_x}{2}\right] = \frac{1}{[\Omega-(1+\lambda_2{}^2)]}\left[\Omega_2 \rho_2^{-\frac{1}{2}} \cos\frac{\phi_2}{2} - (1+\lambda_1{}^2)\rho_1^{-\frac{1}{2}}\cos\frac{\phi_1}{2}\right] \tag{4.73}$$

$$\frac{\partial T}{\partial A_o} = \frac{2\lambda_1}{(\Omega-1-\lambda_2{}^2)}\left(-\rho_2^{-\frac{1}{2}}\sin\frac{\phi_2}{2} + \rho_1^{-\frac{1}{2}}\sin\frac{\phi_1}{2}\right) \tag{4.74}$$

Substituting (4.73) and (4.74) into (4.72), we can get the expression for $\partial G_K/\partial A_o$. Likewise, the partial differentials of G with respect to the other coefficients can be obtained and substituted in eqn. (4.71) to obtain the correction factors for the series constants.

The whole iterative process has been set up in a computer program, written in BASIC. A sizeable number of data points are taken in the isochromatic field and their polar coordinates are fed into the computer with the help of a Calcomp 9000 digitizer. The HP9845A microprocessor is used for computing the series constants iteration after iteration. A listing of the program has been attached in the appendix.

## 4.4 Error Analysis:

The number of coefficients necessary for an adequate representation of the stress field over the data acquisition region can be estimated by examining, as a function of the number of coefficients, the value of the average fringe order error, $|\overline{\Delta n}|$, which is defined in this study as

$$|\Delta n| = \frac{1}{N^*} \sum_{K=1}^{K=N^*} |n_i - n_c|_K \tag{4.75}$$

where $n_i$ is the specified (input) fringe order for a data point, $n_c$ the fringe order calculated from the computed set of coefficients and N* the total number of data points used [12]. Typically, errors of one tenth of a fringe order or less should indicate that the constants are accurate [12].

The error analysis has also been included in the computer program in the appendix.

## 5. EXPERIMENTAL PROCEDURE AND RESULTS

Cross type models were used in this study. The geometry of the specimen is shown in Fig. 7. The specimen length and width were made fairly large to insure that the boundaries were far away from the crack tip as the crack propagated. The starter crack is made with a band saw and the crack tip blunted with a fine file. The model is mounted on the loading frame, shown in Fig. 8, which was so designed that it could be used for both uniaxial and biaxial loading. Loading was applied using ENERPAC hydraulic cylinders and the loads recorded by in-line PCB Model 200A quartz transducers (of Piezotronics, Inc.), used in conjunction with a 484B line power unit. The transducers had built-in ICP (Integrated Circuit Piezoelectric) amplifiers. The cracks were initiated at fairly high loads by means of a solenoid actuated cutting tool so that the $K_Q$ value (stress intensity factor associated with load level Q) lies in the plateau region of the $\dot{a}$-K curve and the crack velocity was close to terminal velocity. Pictures of the propagating crack were taken by the High Speed Recording System and magnified prints were made out of the negatives for analysis. A fairly large number of data points, say 60, were taken on each picture and their locations with respect to the crack tip and crack line were fed into the main analysis program through a Calcomp 9000 digitizer and the series constants obtained.

In Experiment 1, a uniaxial normal stress of 233 psi (1.61 MPa) was applied. The variation of crack tip position with respect to time is shown in Fig. 9. A constant crack velocity of 383 m/s was obtained.

The stress intensity factor, as shown in Fig. 10 and Table 1, showed an increasing trend, values ranging from 1 MPa$\sqrt{m}$ to 1.55 MPa$\sqrt{m}$. The remote stress $\sigma_{ox}$ varied as in Fig. 11 and Table 1, with values oscillating about a mean of -2 MPa.

In Experiment 2, a higher uniaxial normal stress of 558 psi (3.85 MPa] was applied. A crack velocity of 400 m/s was obtained, as shown in Fig. 12. The stress intensity factor showed a sharply increasing trend, as in Fig. 13 and Table 2, with values ranging from 1.1 MPa$\sqrt{m}$ to 1.84 MPa$\sqrt{m}$. The crack started the first of a series of multiple attempts to branch when K was 1.84 MPa$\sqrt{m}$. Thenceforth, the fracture surface was extremely rough with tiny incomplete branches coming out of the crack and the crack finally branched close to the boundary. Because of the belated branching, pictures of actual branching were not recorded. The branching angle was slightly different on the two surfaces, being 24° on one side and 22° on the other. $\sigma_{ox}$ was fairly negative through most of the time because of the forward bend of the loops and it reached up to a maximum of -3.3 MPa, as shown in Fig. 14 and Table 2.

To study the influence of far-field stresses parallel to the crack, a series of biaxial tension-compression and tension-tension experiments were conducted.

Typical isochromatics for tension-compression loading are shown in Fig. 15. It is seen that the fringe loops exhibit a strong forward tilt for this kind of loading, which indicates the nature of the remote parallel stress.

In Experiment 3, a tensile normal stress of 443 psi [3.05 MPa] and a compressive parallel remote stress of 197 psi [1.36 MPa] were applied. The dynamic K was not enough at any stage to produce branching. A con-

stant crack velocity of 368 m/s was obtained, as shown in Fig. 16. Again, K showed an increasing trend as in Fig. 17 and Table 3, with values going up to 1.81 MPa$\sqrt{m}$ and $\sigma_{ox}$ was oscillating about a mild negative mean of -2.1 MPa, as in Fig. 18 and Table 3, with values ranging from -3.4 MPa to 0.4 MPa. The compressive parallel stress was not high enough to produce a sizeable increase in $\sigma_{ox}$. However, the isochromatic fringe loops showed a forward tilt, indicating the nature of the remote parallel stress.

In Experiment 4, a tensile normal stress of 500 psi [3.45 MPa] and a compressive parallel remote stress of 180 psi [1.24 MPa] were applied. Because of the higher normal stress, the crack was initiated at a higher $K_Q$ than Experiment 3. Unfortunately the crack did not branch but there was a conspicuous roughness of the fracture surface in the final stages of crack propagation, showing that the crack would have branched at a slightly higher initial $K_Q$. The K value associated with the roughness of fracture surface was fairly high (1.77 MPa$\sqrt{m}$) as was observed by researchers at the University of Maryland [3] and the University of Washington [15]. Again, K showed a sharply increasing trend with values ranging from 0.98 MPa$\sqrt{m}$ to 1.77 MPa$\sqrt{m}$, as in Fig. 20 and Table 4 and $\sigma_{ox}$ oscillated about a mild negative mean of about -1.3 MPa, as in Fig. 21 and Table 4. The crack velocity was 400 m/s in this experiment and the velocity plot is shown in Fig. 19.

In Experiment 5, the tensile normal stress was increased to 667 psi [4.6 MPa] and the compressive remote parallel stress was 174 psi [1.2 MPa]. The crack branched at a $K_{br}$ of 2.01 MPa$\sqrt{m}$ and K showed an increasing trend as the crack moved across the model, as in Fig. 23 and Table 5. Because of a higher initial $K_Q$, the K values encountered in

this test were fairly high, ranging from 1.7 to 2.01 MPa$\sqrt{m}$. The crack velocity was a constant 385 m/s, as in Fig. 22. $\sigma_{ox}$ values were oscillating about a negative mean of -3.7 MPa as in Fig. 24 and Table 5. The branching angle was 29°.

In Experiment 6, a tensile normal stress of 667 psi [4.6 MPa] and a much higher compressive remote parallel stress of 340 psi [2.34 MPa] were resorted to. For comparison purposes, the tensile normal stress was kept the same as in Experiment 5. It was observed that the K values for the same crack tip positions were lower in this experiment than Experiment 5. $\sigma_{ox}$ reached high negative values up to -9.8 MPa because of a much higher compressive parallel stress, applied in this experiment. The crack velocity plot and the variation of K and $\sigma_{ox}$ with crack tip position are shown in Figures 25, 26 and 27 respectively. K and $\sigma_{ox}$ values are also listed in Table 6. Crack branching occurred at a $K_{br}$ of 1.91 MPa$\sqrt{m}$.

It seems that remote compressive stress parallel to the crack tends to lower the stress intensity factor and hence suppresses branching. In Experiment 5, the crack made an attempt to branch - in fact, it almost branched at a crack jump distance of 7.2 cm, though actual branching occurred at a crack jump distance of 11.8 cm. In Experiment 6, the crack travelled 9.8 cm before it branched. This evidence adds to the fact that compressive remote parallel stress suppresses branching. This was also suggested by Dally et al [2] and Ravichandar [29]. It was also observed in experiments 5 and 6 that the fracture surface roughness was very high either when an attempt was made to branch or when actual branching occurred. Again, the branching angle in Experiment 6 was 24.5° as compared to 29° obtained in Experiment 5, indicating that compressive

parallel remote stress affects the branching angle, though not considerably. The case of compressive $\sigma_{ox}$ has to be studied more by going in for very high compressive parallel loads.

Next, a series of biaxial tension-tension experiments were carried out. Typical isochromatics for this case are shown in Fig. 28. The fringes show a strong backward tilt and exhibit a behavior typical of a DCB specimen. The lean of the fringe patterns again signifies the nature of the remote parallel stress applied.

In Experiment 7, a tensile normal stress of 689 psi [4.75 MPa] and a tensile parallel stress of 240 psi [1.65 MPa] were applied. Even though the normal stress in this experiment was only slightly higher than that in Experiment 6, the K values in this experiment were much higher than the previous experiment for the same crack tip positions. For example at $a^*/w = .38$, K was 1.18 MPa$\sqrt{m}$ in Experiment 6 compared to 1.82 MPa$\sqrt{m}$ in Experiment 7. In fact, the stress intensity factor was so high that the crack branched very early. K varied with crack tip position as in Fig. 30 and Table 7, values starting from 1.81 MPa$\sqrt{m}$. $K_{br}$ was close to 2 MPa$\sqrt{m}$. A crack velocity of 375 m/s was obtained as in Fig. 29. The fracture area before branching was 4.8 $cm^2$ and the branching angle was 30°. These observations point to the fact that tensile remote parallel stress enhances branching, which is in accordance with observations made in explosive testing by Dally et al [2] and Rossmanith and Shukla [30]. $\sigma_{ox}$ values were negative, because the tensile parallel stress was not enough to bend the isochromatic fringes backward. $\sigma_{ox}$ variation is shown in Fig. 31 and Table 7.

In Experiment 8, a tensile normal stress of 422 psi [2.91 MPa] and a tensile parallel stress of 400 psi [2.76 MPa] were applied. Though

the normal stress applied in this test was considerably lower than Experiment 6, the K values for the same crack tip positions in this experiment were higher than Experiment 6, again showing that tensile remote parallel stress enhances the K value, which in turn, enhances branching. In this experiment, branching was not obtained because of an inadequate $K_Q$ at initiation. A constant crack velocity of 377 m/s was obtained as in Fig. 32. K and $\sigma_{ox}$ values varied as in Table 8 and Figures 33 and 34, with K ranging from 1.27 to 1.68 MPa$\sqrt{m}$ and $\sigma_{ox}$ ranging from -2 to 2 MPA with a mean of -.1 MPa. $\sigma_{ox}$ values were less negative than the uniaxial case because of the applied parallel tensile stress but again, the parallel stress was not enough to bend the fringe loops backward sufficiently and hence high positive values were not obtained.

In Experiment 9, a tensile normal stress of 538 psi [3.71 MPa] and a very high tensile parallel stress of 924 psi [6.4 MPa] were applied. A crack velocity of 400 m/s was obtained from Fig. 35. K values were fairly high compared to experiments with compressive $\sigma_{ox}$ and the uniaxial case for the same crack tip locations and comparable initial $K_Q$'s and showed an increasing trend as shown in Table 9 and Fig. 36. The crack branched at a $K_{br}$ value of 1.91 MPa$\sqrt{m}$ and $\sigma_{ox}$ was hovering around high positive values (2.8 to 6 MPa) as in Fig. 37 and Table 9, because of the considerable backward tilt of the fringe loops due to the high parallel stress applied. The branching angle was 73°, which was much higher than the compressive $\sigma_{ox}$ tests. One more interesting comparison can be made between Experiment 9 (normal stress 538 psi and parallel tensile stress 924 psi) and Experiment 2 (uniaxial normal stress 553 psi). In spite of the fact that the applied normal stress

was less in Experiment 9, the K values for the same crack tip locations were much higher in that experiment than Experiment 2, as shown in Tables 2 and 9. As an example, for a*/w = .39, K was 1.56 MPa$\sqrt{m}$ in Experiment 9, compared to 1.28 MPa$\sqrt{m}$ in Experiment 2. The crack jump distance prior to branching was 16.2 cm (fracture area was 17.82 $cm^2$) in Experiment 2 compared to 10.7 cm (fracture area was 10.7 $cm^2$) in Experiment 9. The branching angle was 23° in Experiment 2, compared to 73° in Experiment 9. All these observations point to the fact that tensile parallel remote stress enhances K and hence branching. It also increases the branching angle considerably.

In Experiment 10, a tensile normal stress of 594 psi (4.10 MPa) and a tensile parallel stress of 614 psi (4.23 MPa) were applied. A crack velocity of 380 m/s was obtained and the stress intensity factor at branching was 2 MPa$\sqrt{m}$. The branching angle was 45°. From this experiment, one can conclude that the ratio of the applied normal stress to the applied parallel tensile stress has a marked influence on the branching angle. For the same normal stress, the branching angle increases with the tensile parallel stress. Since branching occurred very early in this experiment, only a few pre-branching pictures were recorded and hence K and $\sigma_{ox}$ variation prior to branching was not plotted.

Stress Intensity Factors at branching, $K_{br}$, branching angles and pre-branching fracture areas for the various experiments are listed in Table 10. $K_{br}$ seems to vary very slightly with different magnitudes of applied stresses and probably depends on initial $K_Q$. More experimentation has to be performed to confirm this. The variation of branching angle and the pre-branching fracture area with respect to

the ratio of the applied normal stress to the applied parallel stress ($\sigma_y/\sigma_x$) is shown in Figures 38 and 39 respectively, just to highlight the facts that branching occurs earlier in the case of positive $\sigma_{ox}$, even with lower normal stresses, compared to the uniaxial and the tensile-compressive cases and that branching angles are much higher in the tensile-tensile case.

The isochromatics for uniaxial, tensile-compressive and tensile-tensile cases are compared in Fig. 40 to explicitly show the slight forward tilt of the loops in the uniaxial case and the considerable backward and forward tile in the tensile-tensile and tensile-compressive cases respectively.

The crack velocities and K-values, encountered in various experiments are plotted in Fig. 41. The points form a fairly narrow band in the high velocity region, with velocities ranging from 370 m/s to 400 m/s. The remote parallel stress does not seem to have any major or well-defined influence on the crack velocity.

Photographs of the tested specimens for the experiment 2 (uniaxial normal stress of 558 psi), experiment 5 (normal tensile stress of 667 psi and parallel compressive stress of 174 psi), experiment 9 (normal tensile stress of 538 psi and parallel tensile stress of 924 psi) and experiment 10 (normal tensile stress of 594 psi and parallel tensile stress of 614 psi) are given in Figures 42, 43, 44 and 45 respectively to show the branching angles obtained.

## 6. CONCLUSION

A photoelastic investigation of high speed crack propagation and branching was performed for cross-type specimens fabricated from Homalite 100 under uniaxial and biaxial loading conditions. Special consideration was given to the variation of the singular and non singular stress field coefficients as the crack propagated through the model. The effect of remote parallel stress $\sigma_{ox}$ on crack propagation and branching was studied by applying very high tensile and compressive stresses parallel to the crack. The stress intensity factor showed an increasing trend as the crack propagated in the models. The value of K increased till crack branching was achieved. The branching stress intensity factor $K_{br}$ was found to vary slightly with $K_Q$ at initiation and the nature of the remote parallel stress. Branching angles in tensile $\sigma_{ox}$ experiments were as high as 73°, compared to values between 22° and 29° encountered in compressive $\sigma_{ox}$ and uniaxial cases, which point to the fact that tensile remote parallel stress increases the branching angle considerably. It was also observed that higher compressive $\sigma_{ox}$ lowers the branching angle, though not sizably, for the same normal stress applied. This was evident from the branching angle of 24.5° obtained in Expt. 6 (normal stress 667 psi and parallel stress 340 psi) as compared to 29° obtained in Expt. 5 (normal stress 667 psi and parallel stress 174 psi). More experimentation has to be done to confirm the effect of compressive $\sigma_{ox}$.

Again, the pre-branching fracture area was higher in the compressive

$\sigma_{ox}$ cases than that in all the tensile-tensile experiments, signifying that tensile $\sigma_{ox}$ tends to enhance branching and compressive $\sigma_{ox}$ tends to suppress it. Also, tensile $\sigma_{ox}$ gives rise to higher stress intensity factors in comparison to the compressive case for the same crack tip positions and comparable $K_Q$ values, which in turn, favors branching. A high roughness of fracture surface was associated with branching or attempts to branch.

Ramulu et al [15] have formulated a criterion for crack branching which says that a necessary and sufficient condition for branching is a crack branching stress intensity factor $K_{Ib}$, accompanied by a minimum characteristic distance $r_o = r_c$, which is a material property. They have also used equations for $r_o$ and crack curving angle $\theta_c$ which are as follows:

$$r_o = \frac{1}{128\pi} \left[\left(\frac{K_I}{\sigma_{ox}}\right) f(c,c_1,c_2)\right]^2 \qquad (6.1)$$

$$\theta_c = \cos^{-1}\{ f[\left(\frac{\sigma_{ox}}{K_I}\right)^2, r_o]\} \qquad (6.2)$$

In this work, $r_o$ was calculated for the various branching situations and the values, which ranged from 1.1 to 8.1 mm, were found to differ considerably from the $r_c$ value of 1.3 mm, obtained by Ramulu and co-workers. The $r_o$ values are shown in Table 11. Also, the branching angle was found to be dependent on the sign of $\sigma_{ox}$, i.e. the nature of the remote parallel stress, in contradiction to the equation (6.2), used by Ramulu et al, which seems to signify that the angle is independent of the sign of $\sigma_{ox}$.

This study concludes that high velocity crack propagation and crack branching are considerably influenced by non-singular stress field co-

efficients. More investigation has to be carried out to formulate an empirical branching criterion in terms of K, the crack velocity $\dot{a}$ and higher order stress field coefficints.

In this juncture, it has to be mentioned that the branching angles obtained were the macroscopic angles measured just at the crack tip. The branches tend to attract or repel each other, as was observed by Kalthoff [19], which makes it difficult to measure the exact macroscopic branching angle.

It was also observed that the results obtained by the crack tip stress analysis procedure, outlined in Chapter 4, are sensitive to all the input parameters including the radius, theta and the fringe order of the data points. For some unknown reason, there was a convergence problem in the six parameter model when the remote parallel stress was compressive. This was not the case when it was tensile or when uniaxial normal loads were applied.

## REFERENCES


1. Irwin, G.R. et al, "On the Determination of the $\dot{a}$-K Relationship for Birefringent Polymers," Experimental Mechanics, Vol. 19, No. 4, pp. 121-128, April 1979.

2. Dally, J.W., "Dynamic Photoelastic Studies of Fracture," Experimental Mechanics, Vol. 19, No. 10, pp. 349-361, October 1979.

3. Rossmanith, H.P. and Irwin, G.R., "Analysis of Dynamic Isochromatic Crack Tip Stress Patterns," University of Maryland Report.

4. Kobayashi, A.S. et al, "Crack Branching in Homalite 100 Sheets," Engg. Fracture Mechanics, Vol. 6, pp 81-92, 1974.

5. Post, D., "Photoelastic Stress Analysis for an Edge Crack in a Tensile Field," Proc. of SESA, 12(1), pp. 99-116 (1954).

6. Wells, A. and Post, D., "The Dynamic Stress Distribution Surrounding a Running Crack - A Photoelastic Analysis," Proc. of SESA, 16(1), pp. 69-92 (1958).

7. Irwin, G.R., "Discussion of Reference 6," Proc. of SESA, 16(1), pp. 93-96 (1958).

8. Dixon, J.R., "Stress and Strain Distributions around Cracks in Sheet Materials Having Various Work Hardening Characteristics," Intl. Journal of Fracture Mechanics, 1(3), pp. 224-244 (1965).

9. Gerberich, W., "Stress Distribution about a Slowly Growing Crack determined by the Photoelastic-Coating Technique," Experimental Mechanics, 2(12), pp. 359-365 (1962).

10. Schroedl, M.A., McGowen, J.J. and Smith, C.W., "Assessment of Factors Influencing Data Obtained by the Photoelastic Stress Freezing Technique for Stress Fields near Crack Tips," Journal of Engg. Fract. Mechanics, 4(4), pp. 801-809 (1972).

11. Kobayashi, T. and Dally, J.W., "A System of Modified Epoxies for Dynamic Photoelastic Studies of Fracture," Experimental Mechanics, 17(10), pp. 367-374 (1977).

12. Sanford, R.J. et al, "A Photoelastic Study of the Influence of Non-Singular Stresses in Fracture Test Specimens," University of Maryland Report, p. 1, Aug. 1981.

13. Irwin, G.R., "Constant Speed Semi-Infinite Tensile Crack Opened by a Line Force, P, at a Distance, b, from the Leading Edge," Lehigh University Lecture Notes.

14. Sanford, R.J. and Dally, J.W., "A General Method for Determining Mixed Mode Stress Intensity Factors from Isochromatic Fringe Patterns," J. of Engr. Fract. Mech., 11, 621-633 (1979).

15. Ramulu, M. et al, "Dynamic Crack Branching - A Photoelastic Evaluation," ONR Technical Report No. UWA/DME/TR-82/43.

16. Yoffe, E.H., "The Moving Griffith Crack," Philosophical Magazine, Series 7, 42, 739 (1951).

17. Craggs, J.W., "On the Propagation of a Crack in an Elastic Brittle Material," J. Metals Phy. Solids, Vol. 8, pp. 66-75, 1960.

18. Clark, A.B.J., and Irwin, G.R., "Crack Propagation Behaviors," Exp. Mech. 6, 321-330, 1966.

19. Kalthoff, J.F., "On the Propagation Direction of Bifurcated Cracks," Proc. of "Dynamic Crack Propagation," (ed. G.C. Sih), Lehigh University, Noordhoff Int. Publishing, pp. 449-458, 1972.

20. Anthony, S.R. and Congleton, J., "Crack Branching in Strong Metals," Metals Science, Vol. 2, pp. 158-160, 1968.

21. Congleton, J., "Practical Applications of Crack Branching Measurements," Proc. of Dynamic Crack Propagation (ed. G.C. Sih) Lehigh University; Noordhoff Int. Publishing, 1972.

22. Doll, W., "Investigations of the Crack Branching Energy," Int. J. of Fracture, 11, 184, 1975.

23. Kirchner, H.P., "The Strain Intensity Criterion for Crack Branching in Ceramics," Eng. Frac. Mech., Vol. 10, pp. 283-288, 1978.

24. Rossmanith, H.P., "Crack Branching in Brittle Materials - Part I," University of Maryland Report 1977-80.

25. Cranz, C. and Schardin, H., Zeits. f. Phys., 56, 147-83, 1929.

26. Dally, J.W. and Riley, W.F., "Experimental Stress Analysis," McGraw-Hill, p. 406, 1978.

27. Shukla, A., "Crack Propagation in Ring Type Fracture Specimens," M.S. Thesis, University of Maryland, p. 50, 1978.

28. Irwin, G.R. et al, "A Photoelastic Characterization of Dynamic Fracture," Univ. of Maryland Report, pp. 87-93, Dec. 1976.

29. Ravi Chandar, K., "An Experimental Investigation into the Mechanics of Dynamic Fracture," Ph.D. Thesis, California Inst. of Tech., pp. 124, 1982.

30. Rossmanith, H.P. and Shukla, A., "Dynamic Photoelastic Investigation of Interaction of Stress Waves with Running Cracks," Exp. Mech., pp. 415-422, Nov. 1981.

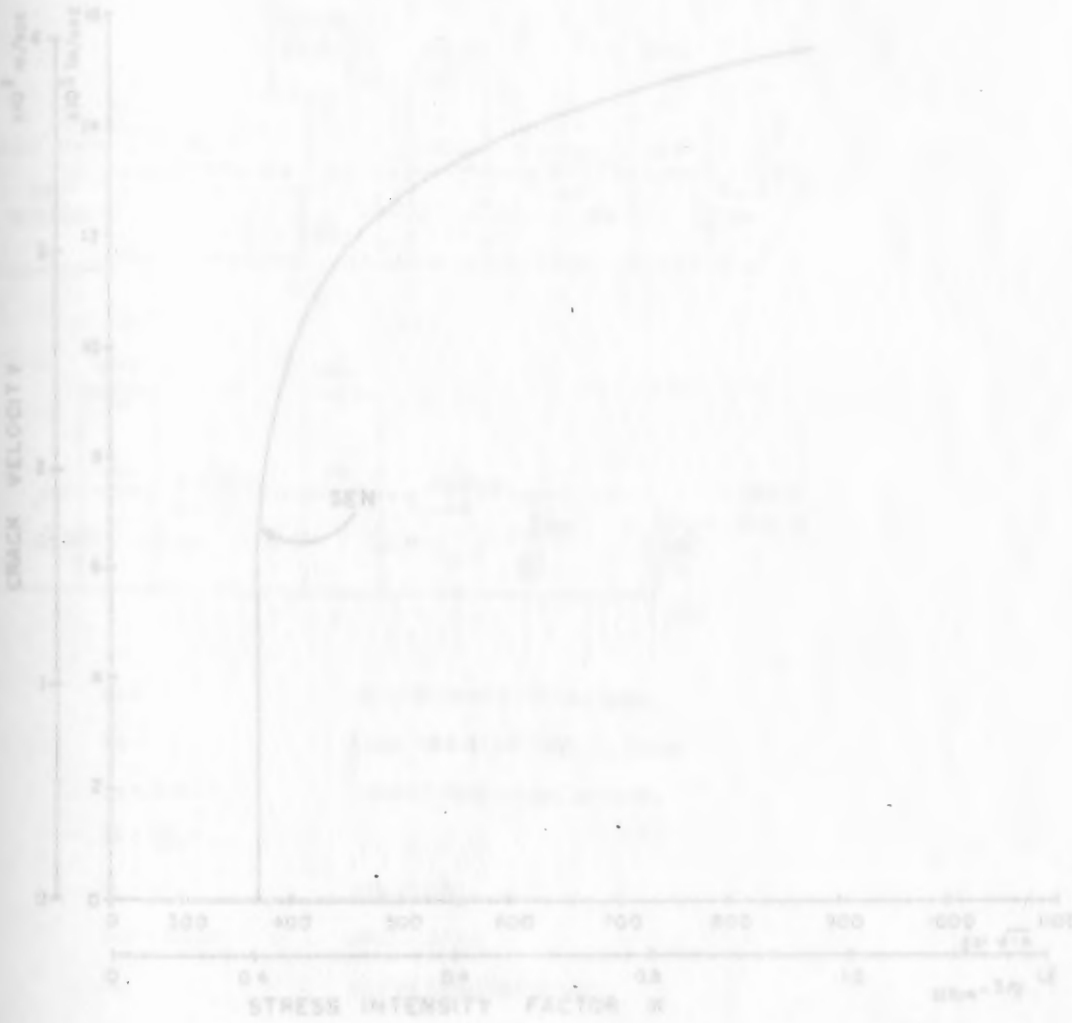

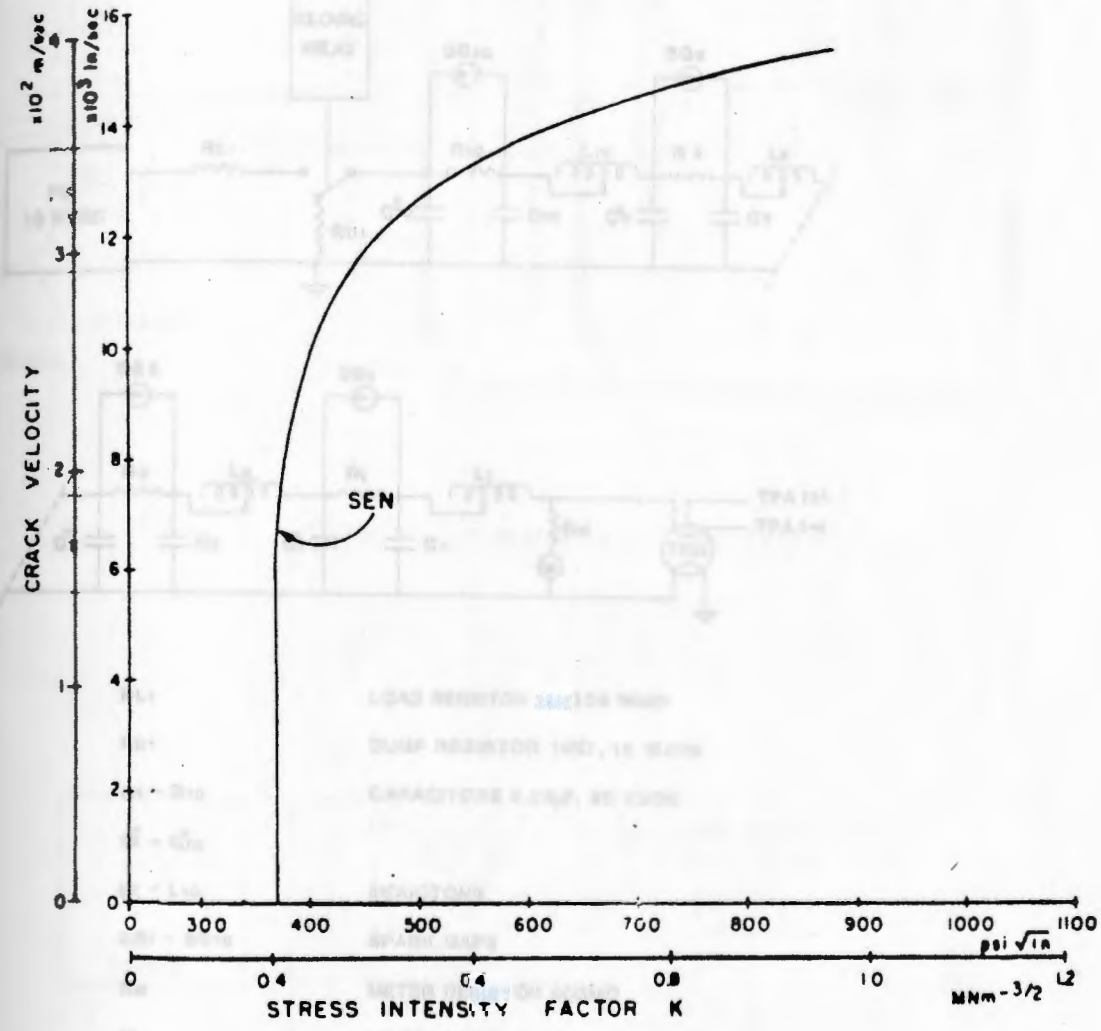


FIG. 1. Typical $\dot{a}$ - K Curve for Homalite 100.

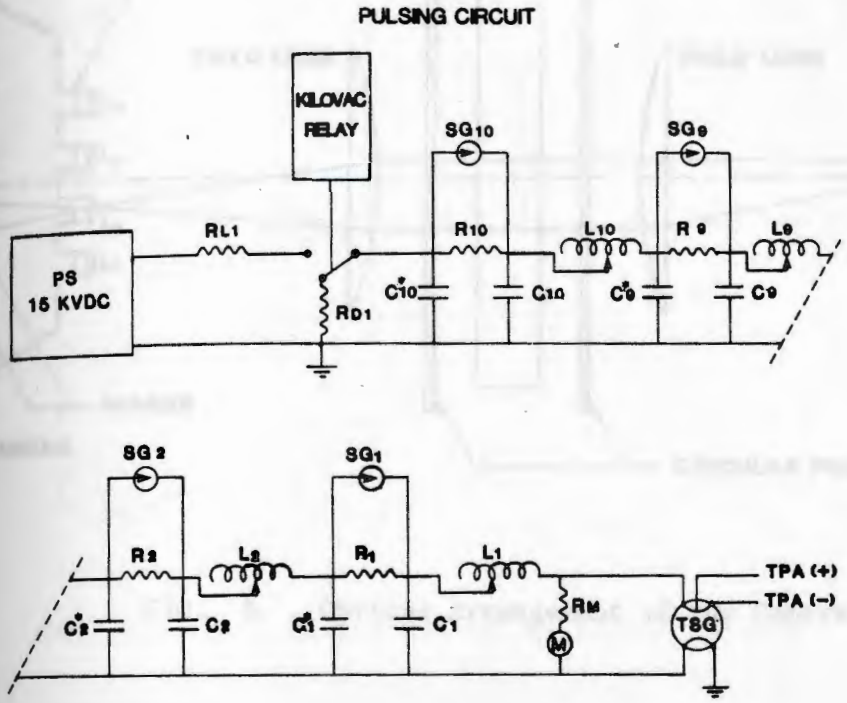


| | |
|---|---|
| $R_{L1}$ | LOAD RESISTOR 3MΩ 24 Watts |
| $R_{D1}$ | DUMP RESISTOR 1MΩ, 16 Watts |
| $C_1 - C_{10}$ | CAPACITORS 0.05μF, 20 KVDC |
| $C_1^* - C_{10}^*$ | |
| $L_1 - L_{10}$ | INDUCTORS |
| $SG_1 - SG_{10}$ | SPARK GAPS |
| $R_M$ | METER RESISTOR 400MΩ |
| M | METER 0-50μA |
| TSG | TRIGGER SPARK GAP |
| $R - R_{10}$ | BLEED RESISTORS 2MΩ |

FIG. 2. Pulsing Circuit of the Camera.

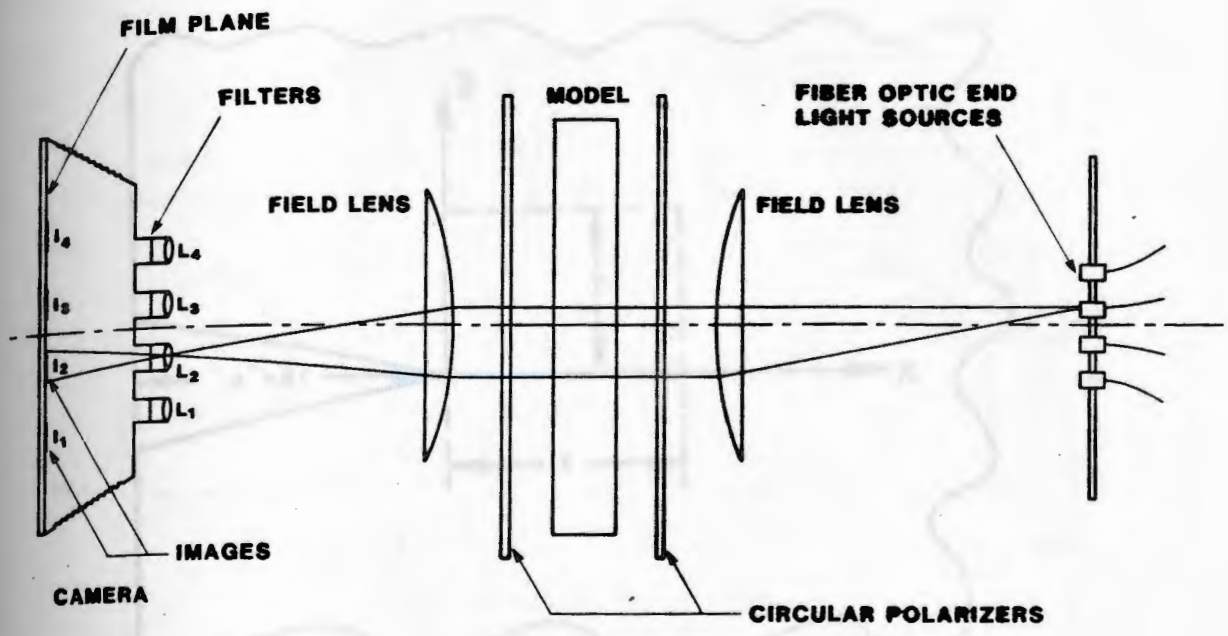


FIG. 3. Optical Arrangement of the Camera.

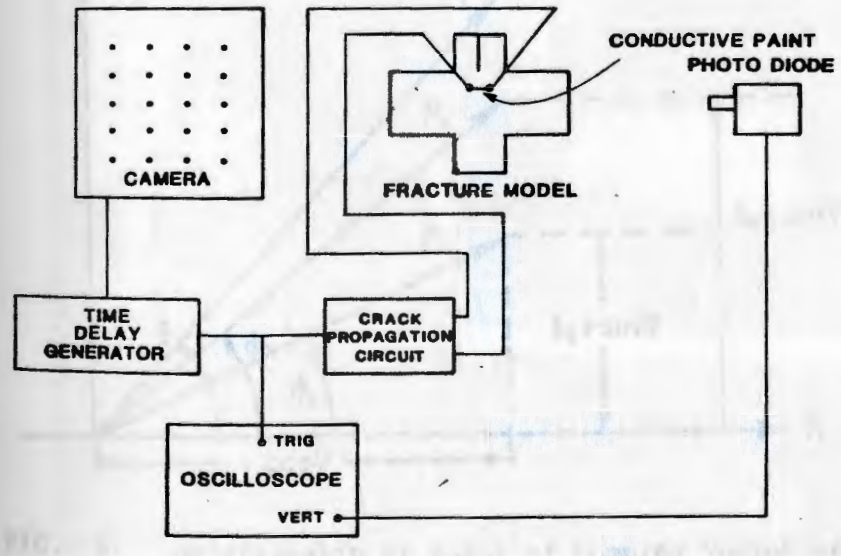


FIG. 4. Schematic Diagram for the Synchronization Circuits.

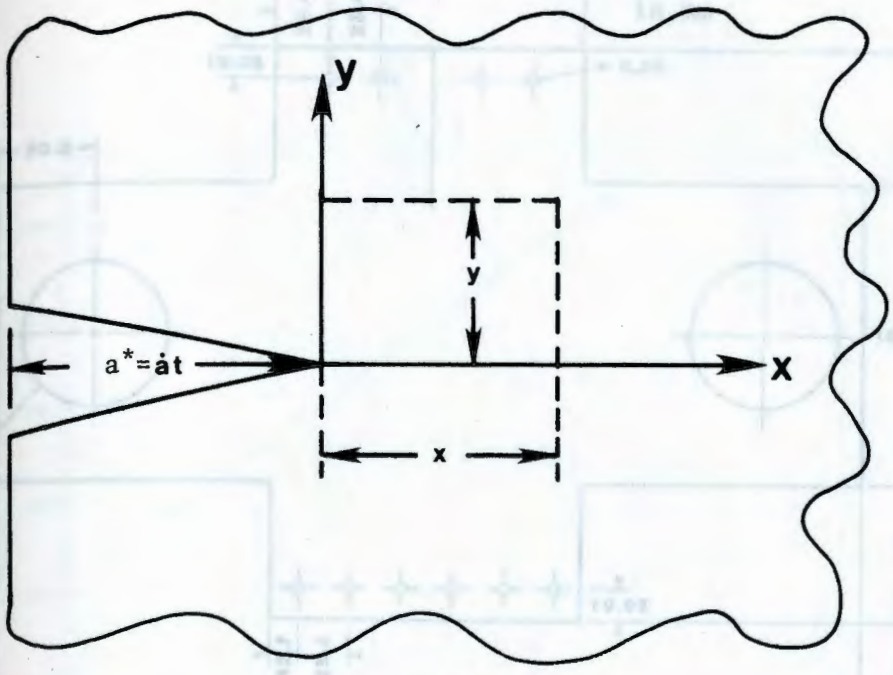


FIG. 5. Co-ordinate System for Crack Tip Stress Analysis.

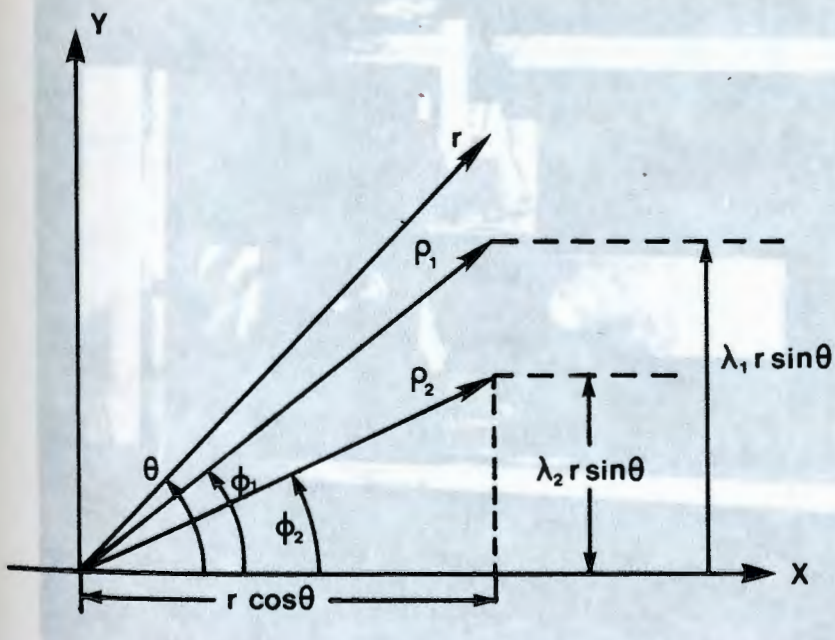


FIG. 6. Relationship of Radii of Complex Variables of the Stress Functions.

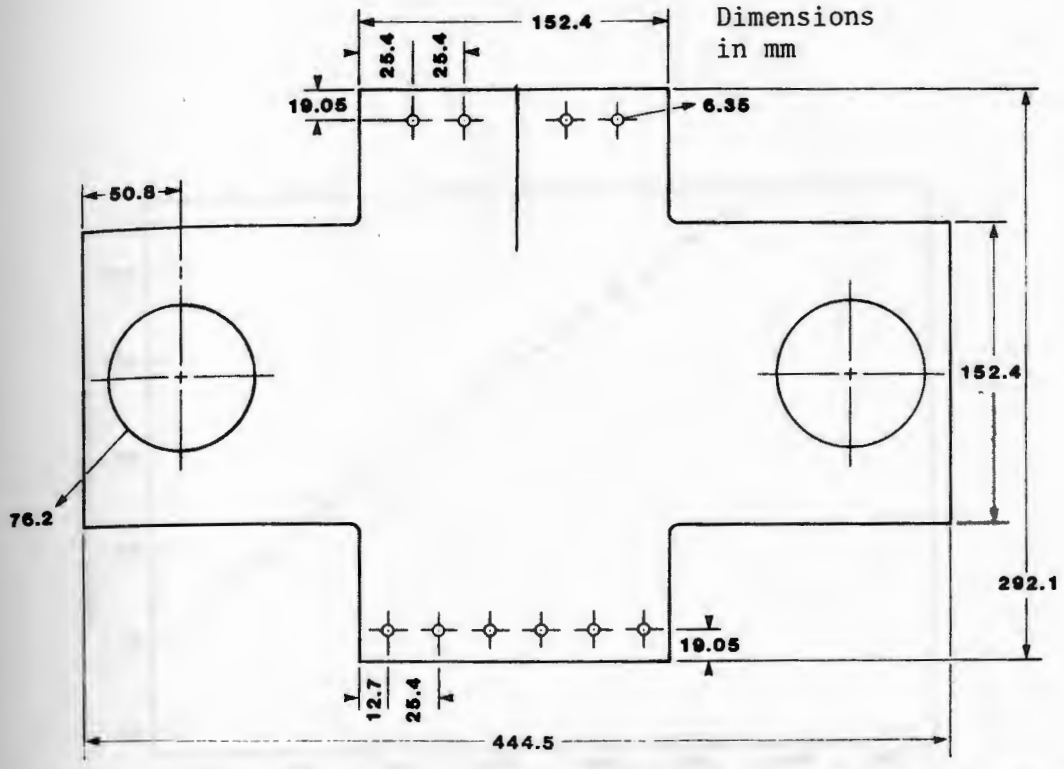


FIG. 7. Specimen Geometry for Biaxial Tension-Tension Loading

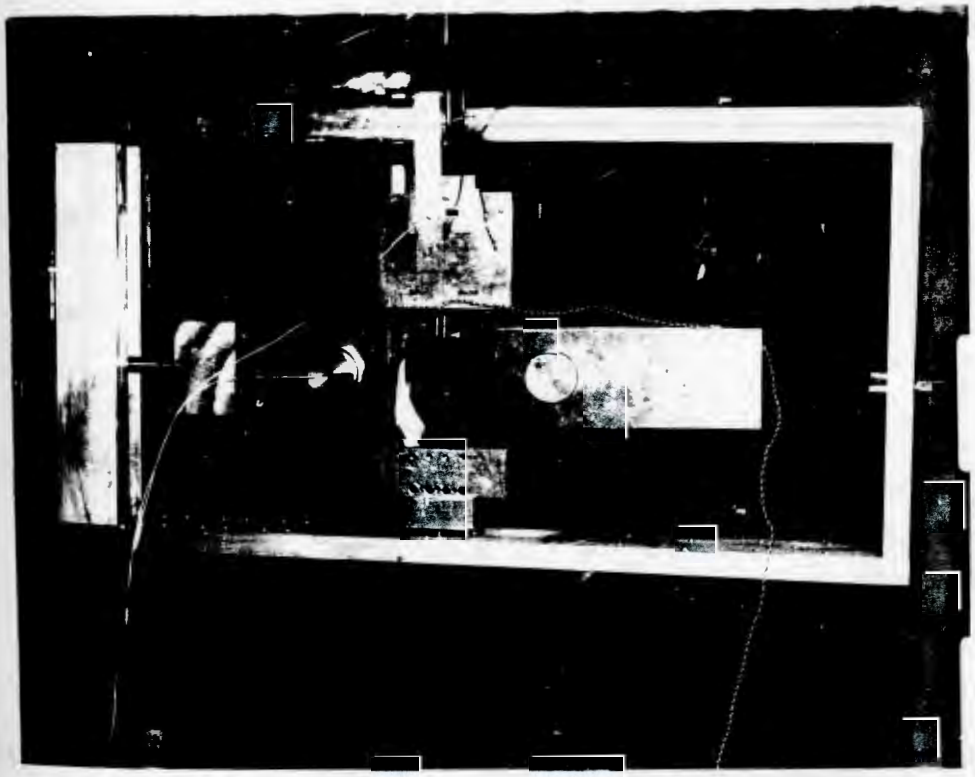

FIG. 8. Loading Frame for Experimentation.

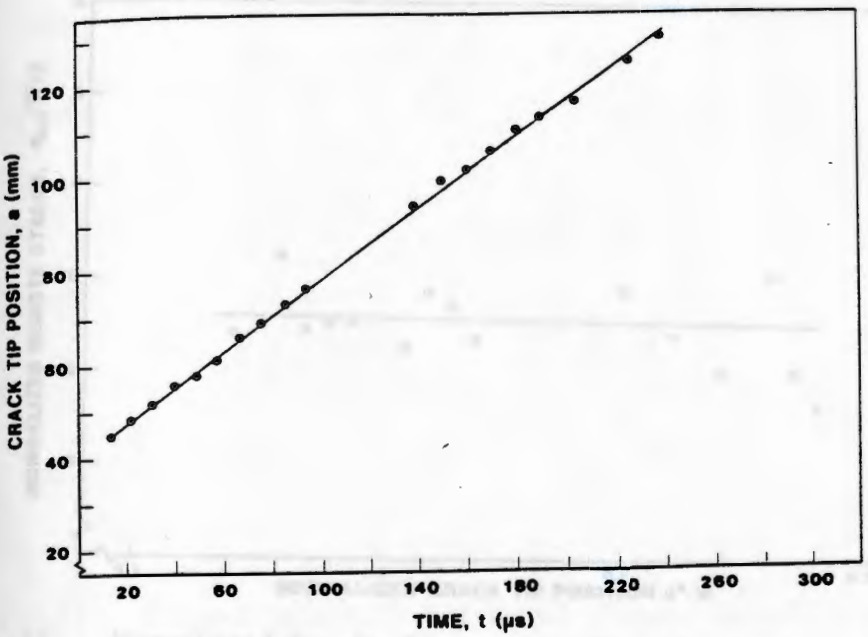


FIG. 9. Crack Extension vs. Time Plot for Experiment 1.

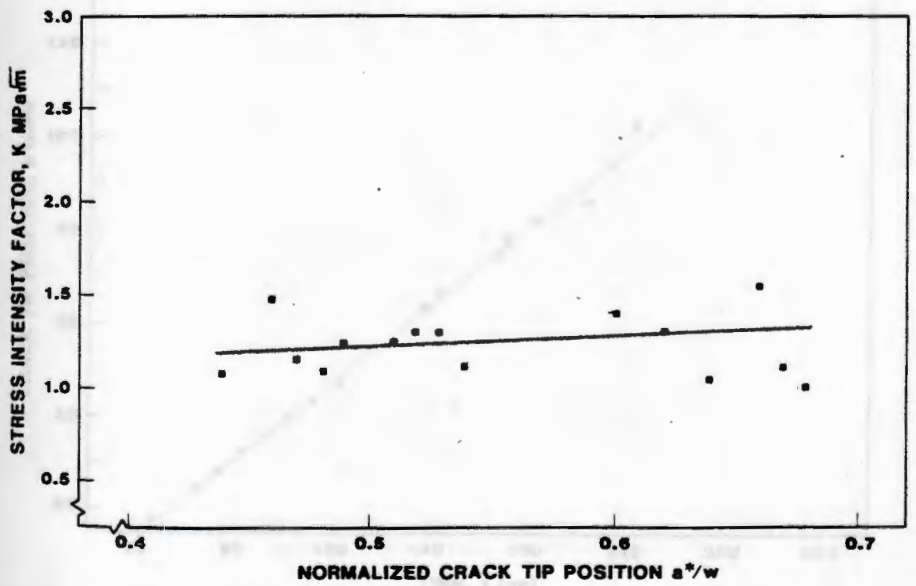


FIG. 10. Stress Intensity Factor as a Function of Normalized Crack Tip Position for Experiment 1.

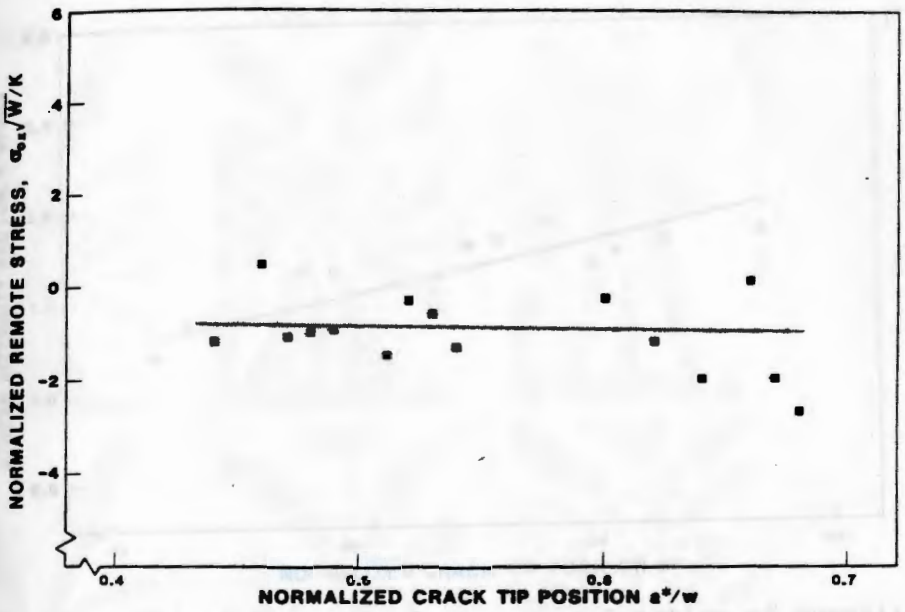


FIG. 11. Normalized Remote Stress as a Function of Normalized Crack Tip Position for Experiment 1.

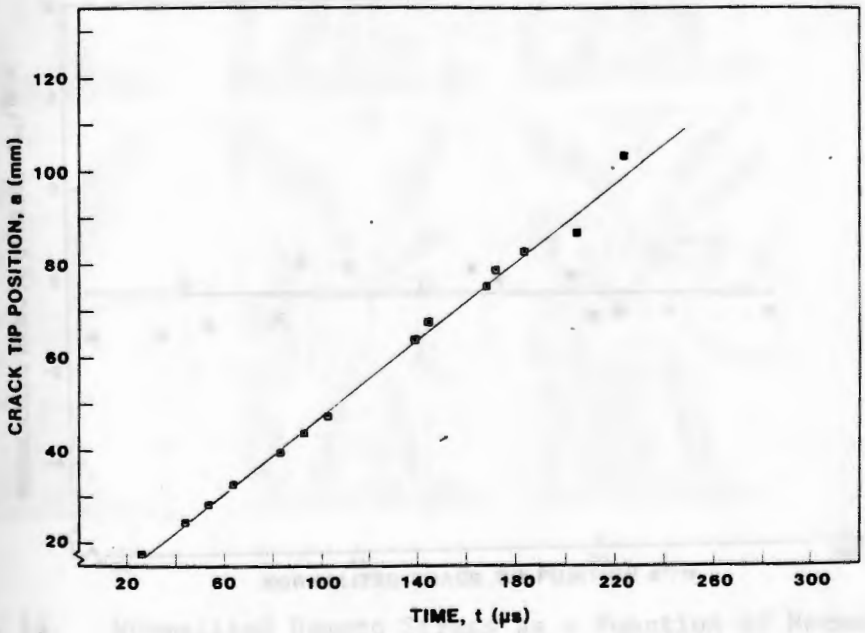


FIG. 12. Crack Extension vs. Time Plot for Experiment 2.

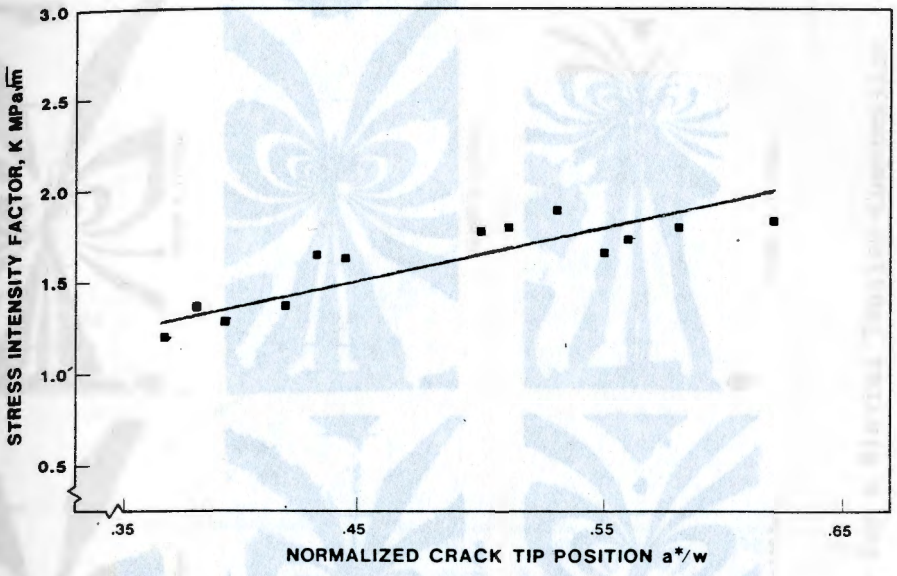


FIG. 13. Stress Intensity Factor as a Function of Normalized Crack Tip Position for Experiment 2.

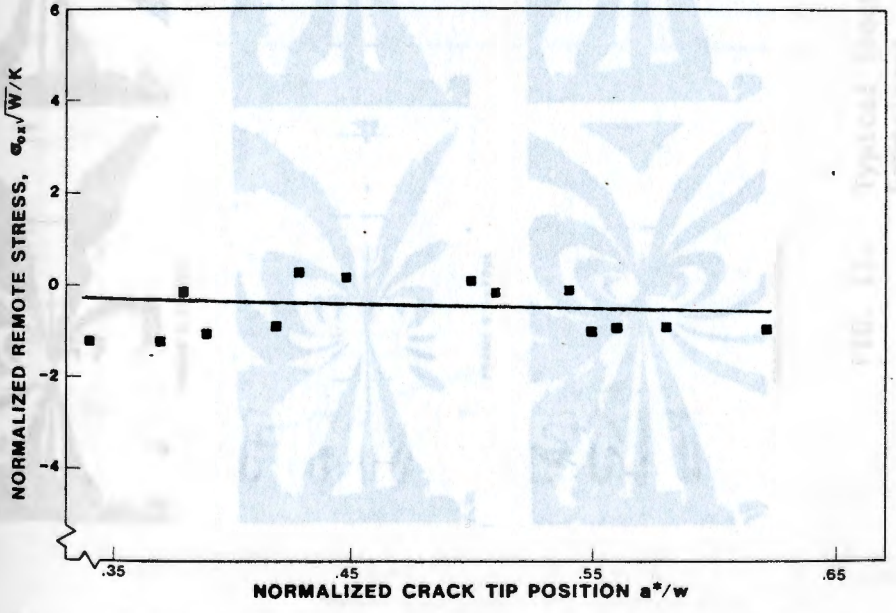


FIG. 14. Normalized Remote Stress as a Function of Normalized Crack Tip Position for Experiment 2.

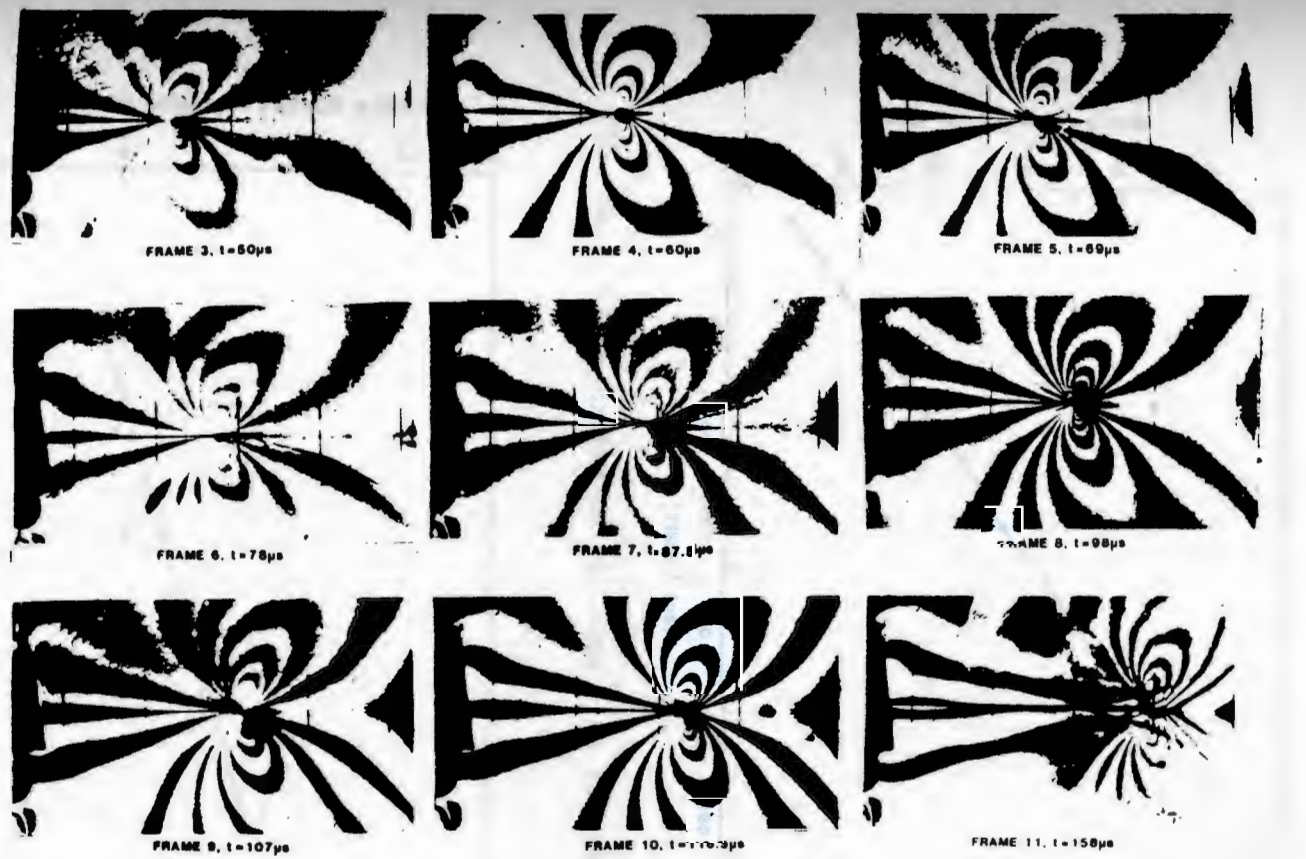


FIG. 15. Typical Isochromatics for a Biaxial Tension-Compression Experiment.

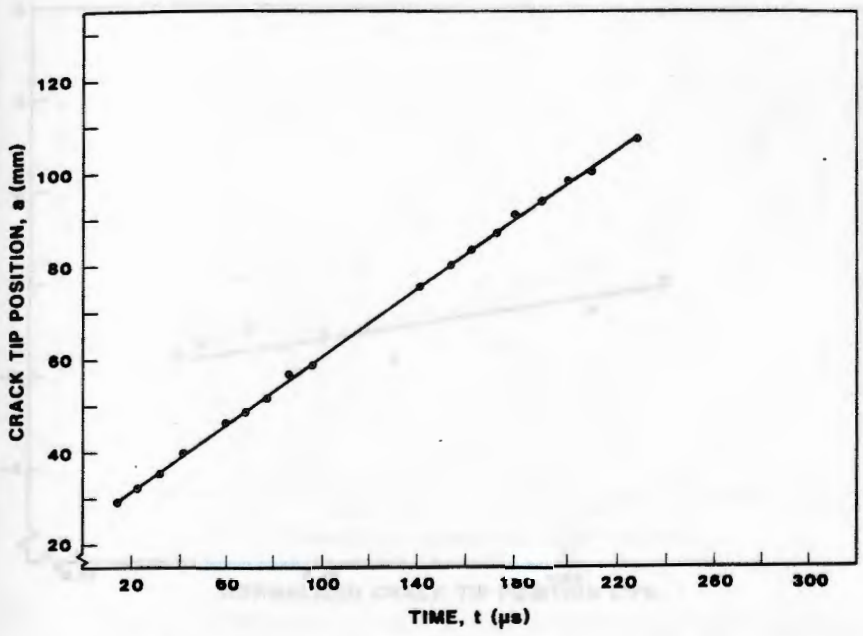


FIG. 16. Crack Extension vs. Time Plot for Experiment 3.

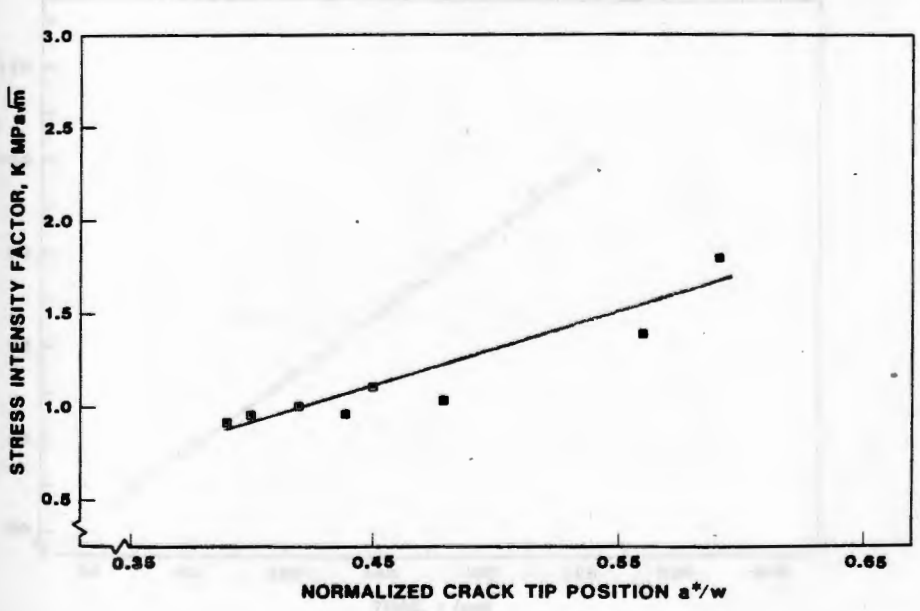


FIG. 17. Stress Intensity Factor as a Function of Normalized Crack Tip Position for Experiment 3.

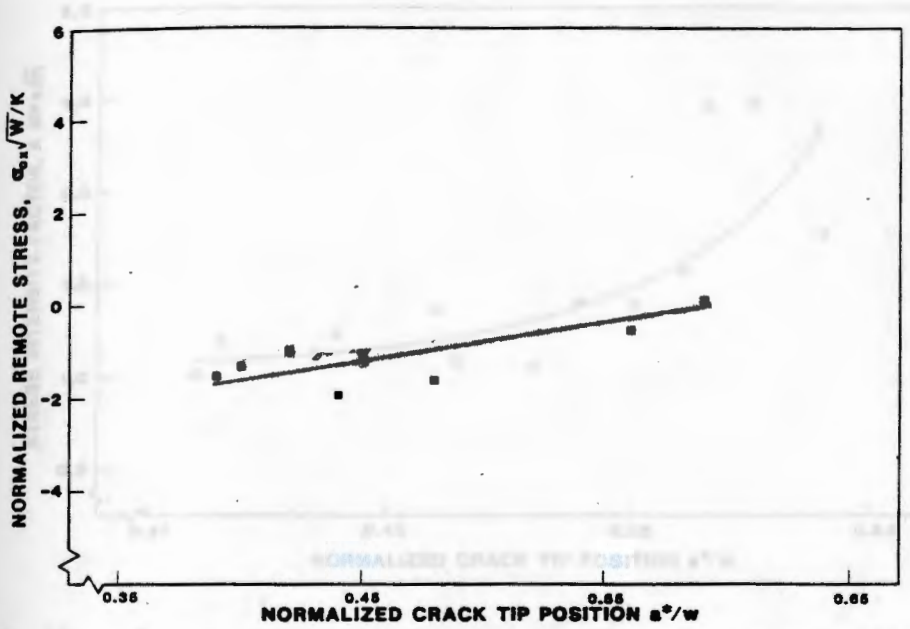


FIG. 18. Normalized Remote Stress as a Function of Normalized Crack Tip Position for Experiment 3.

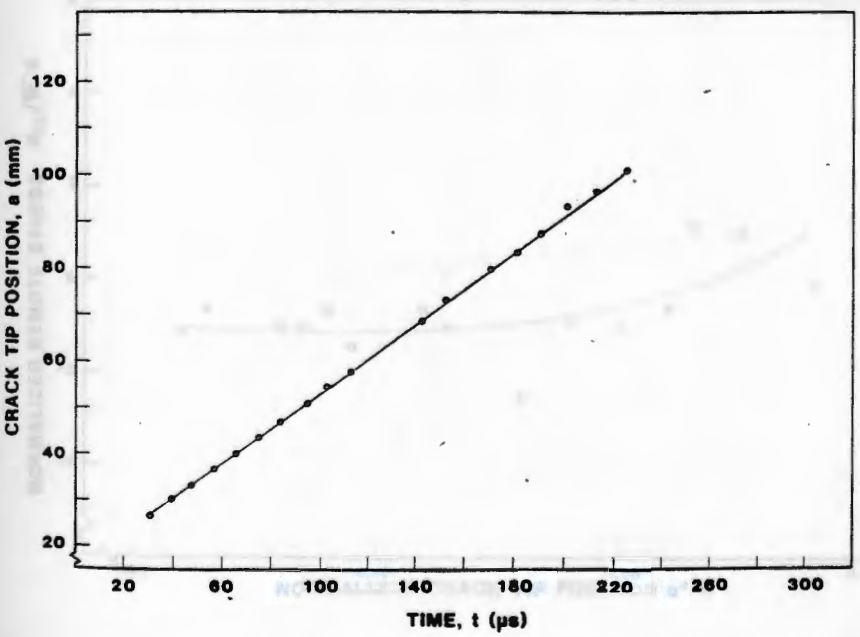


FIG. 19. Crack Extension vs. Time Plot for Experiment 4.

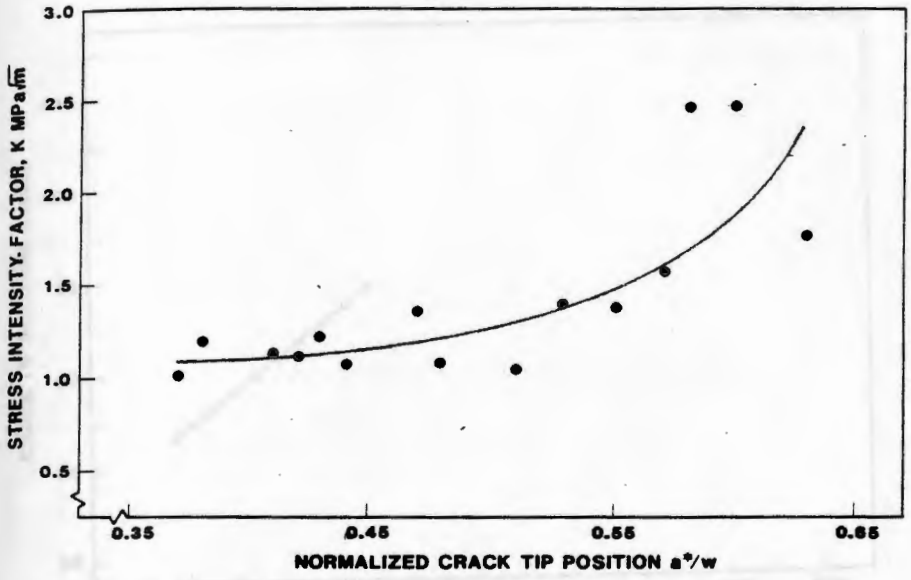


FIG. 20. Stress Intensity Factor as a Function of Normalized Crack Tip Position for Experiment 4.

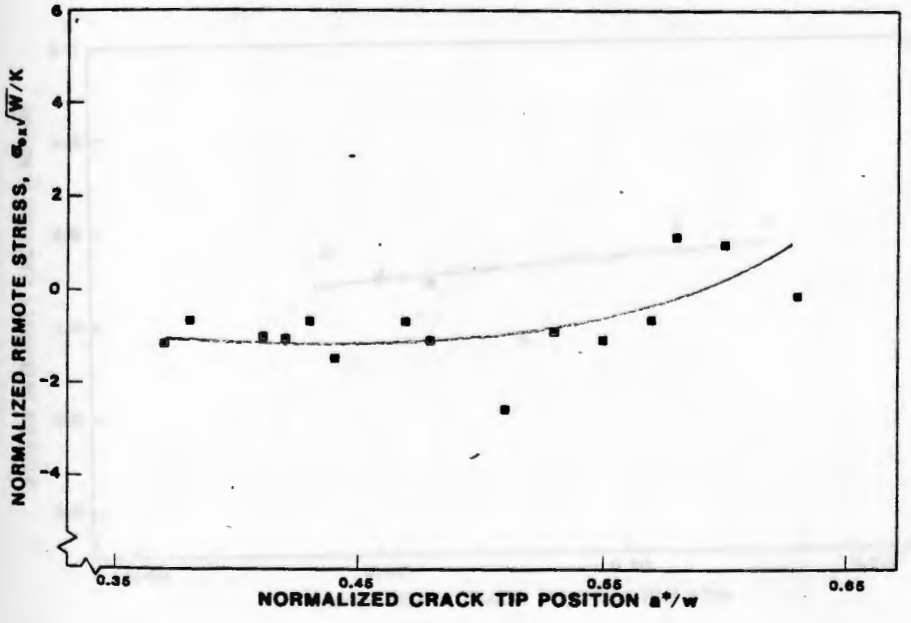


FIG. 21. Normalized Remote Stress as a Function of Normalized Crack Tip Position for Experiment 4.

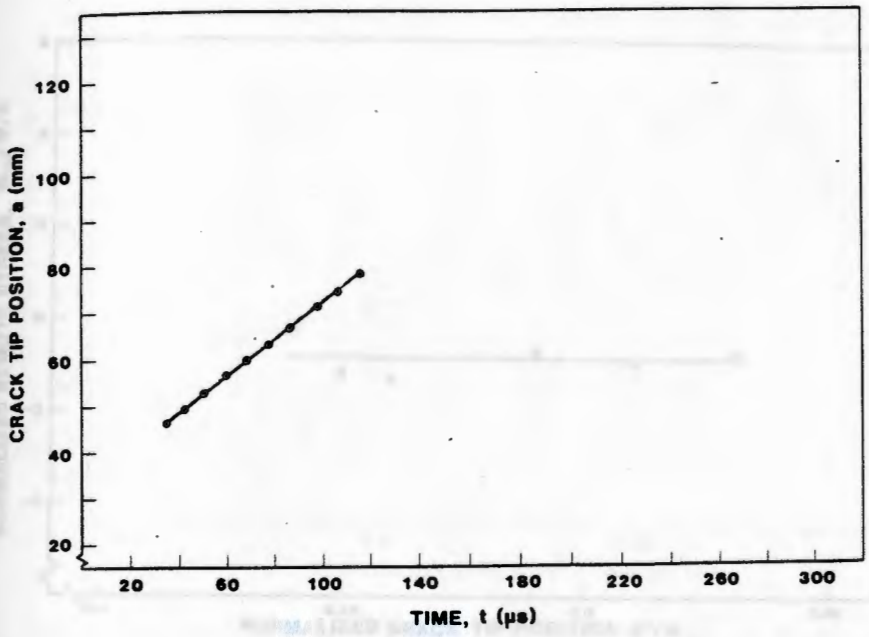


FIG. 22. Crack Extension vs. Time Plot for Experiment 5.

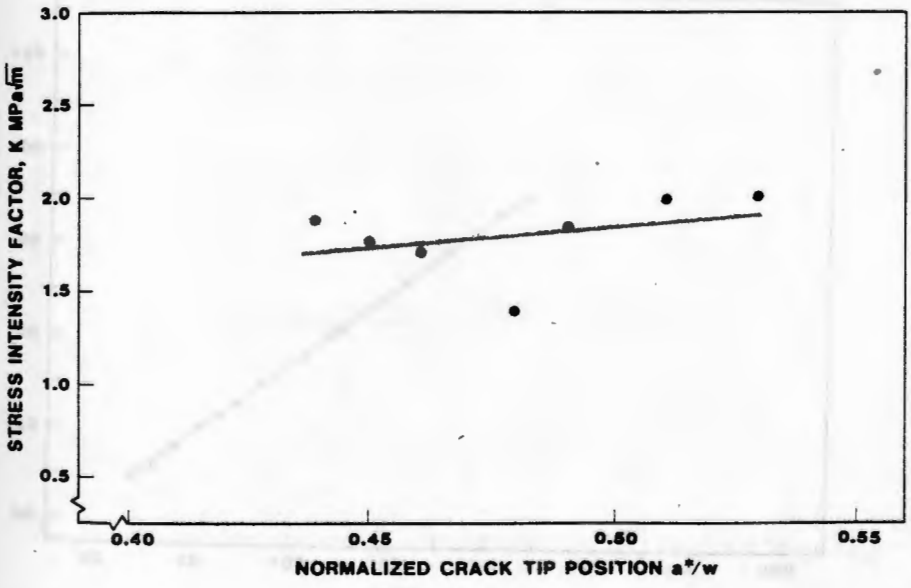


FIG. 23. Stress Intensity Factor as a Function of Normalized Crack Tip Position for Experiment 5.

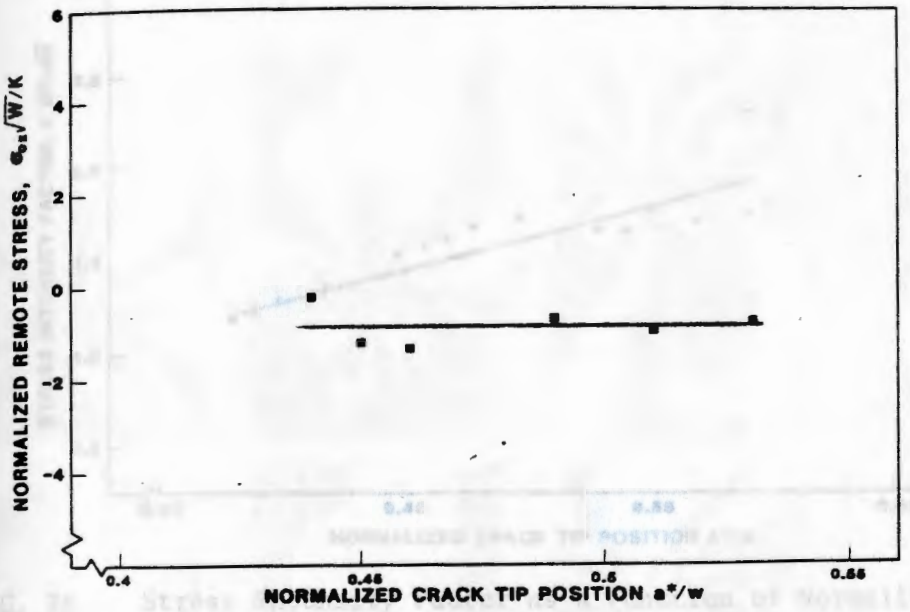


FIG. 24. Normalized Remote Stress as a Function of Normalized Crack Tip Position for Experiment 5.

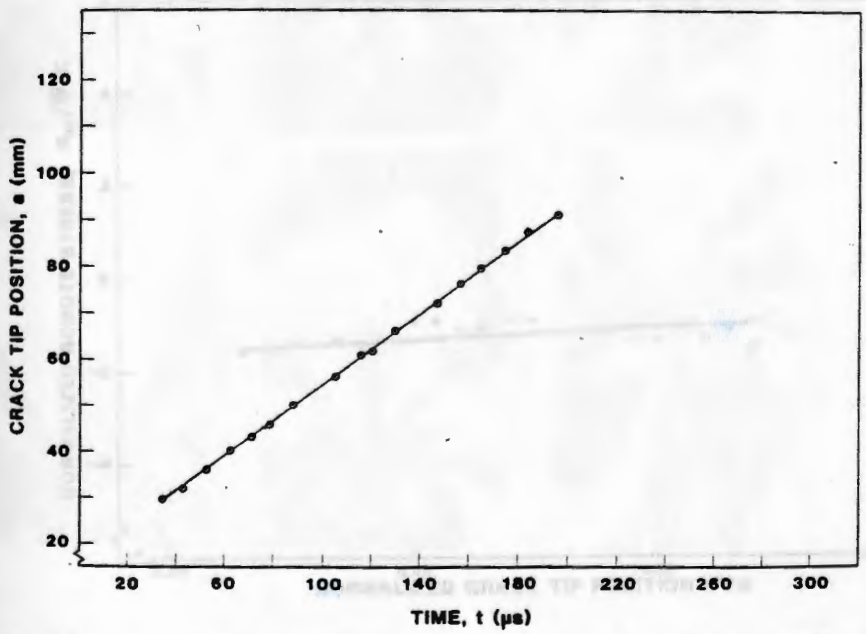


FIG. 25. Crack Extension vs. Time Plot for Experiment 6.

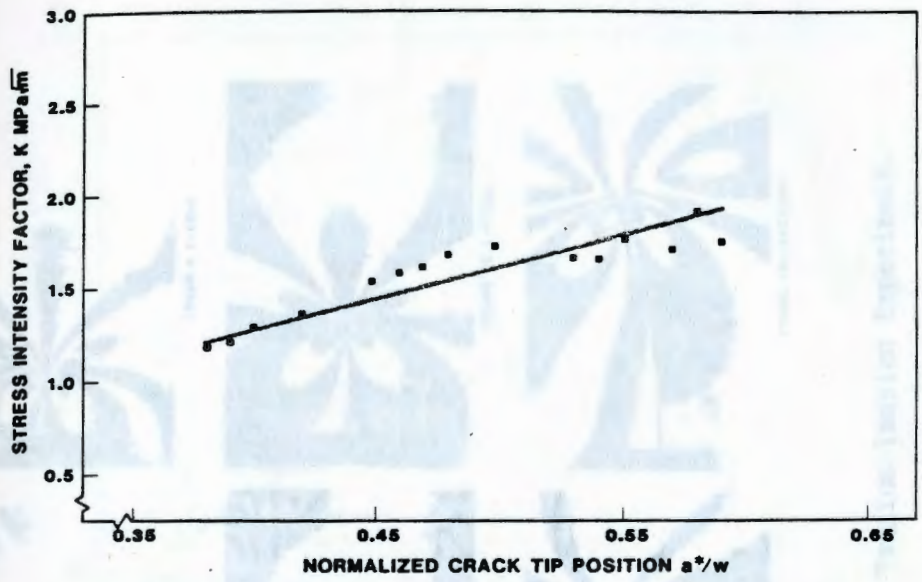


FIG. 26. Stress Intensity Factor as a Function of Normalized Crack Tip Position for Experiment 6.

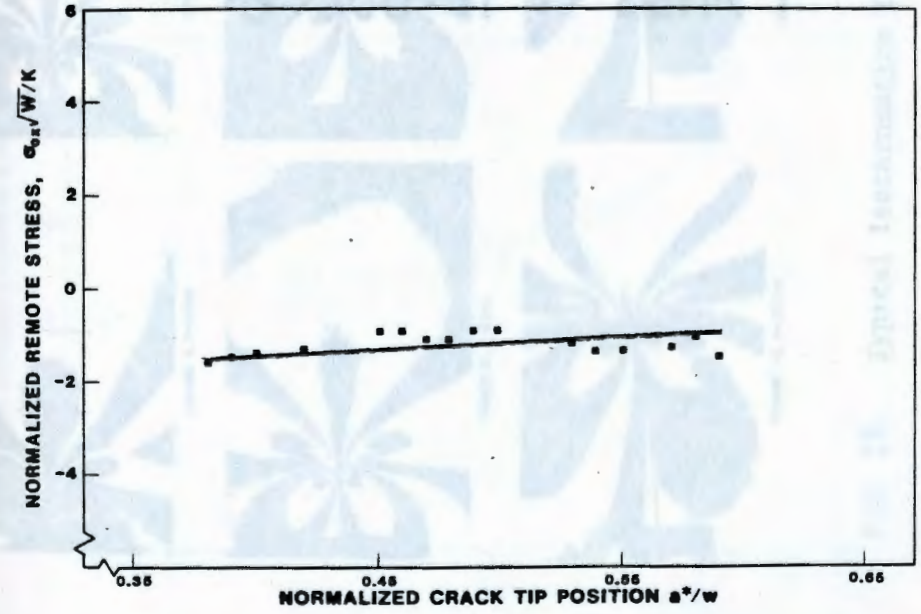


FIG. 27. Normalized Remote Stress as a Function of Normalized Crack Tip Position for Experiment 6.

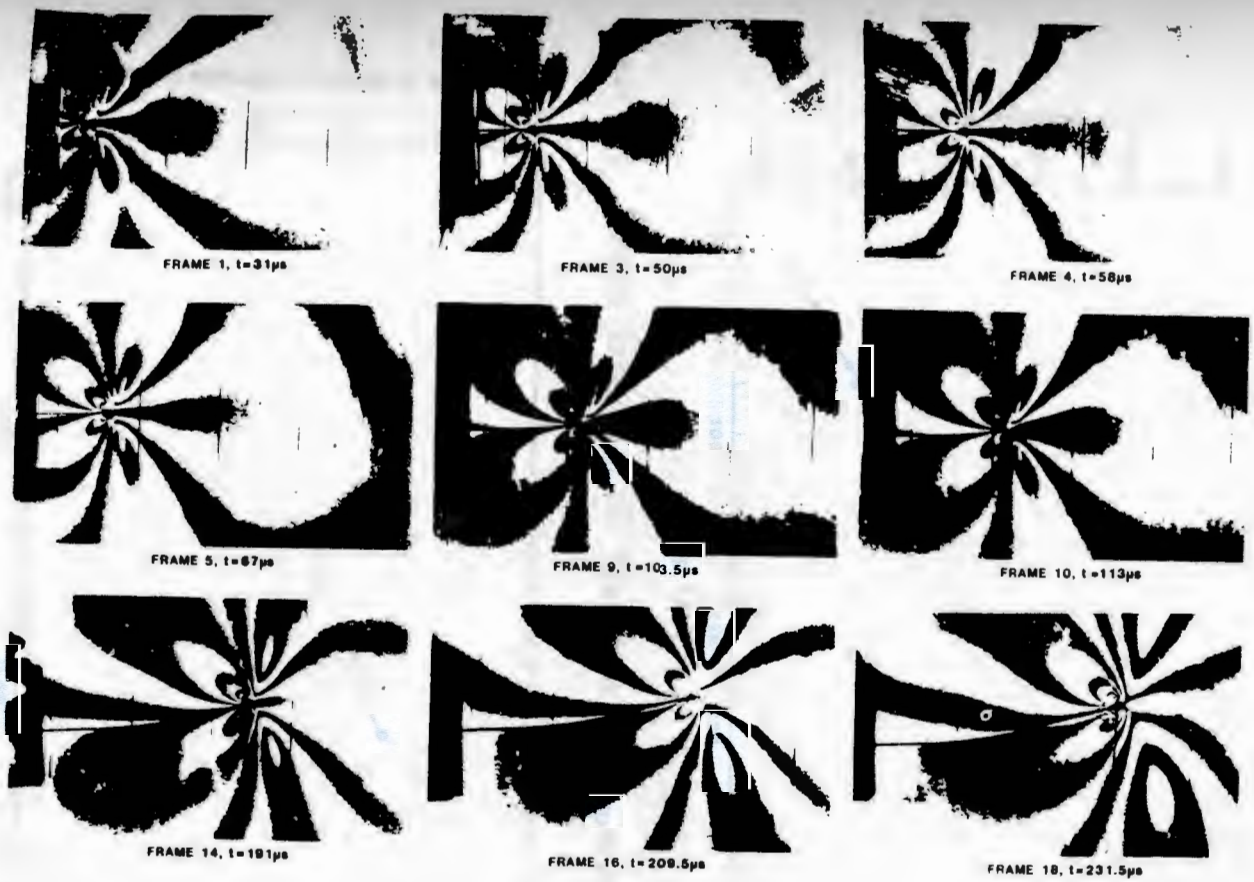


FIG. 28. Typical Isochromatics for Biaxial Tension-Tension Experiment.

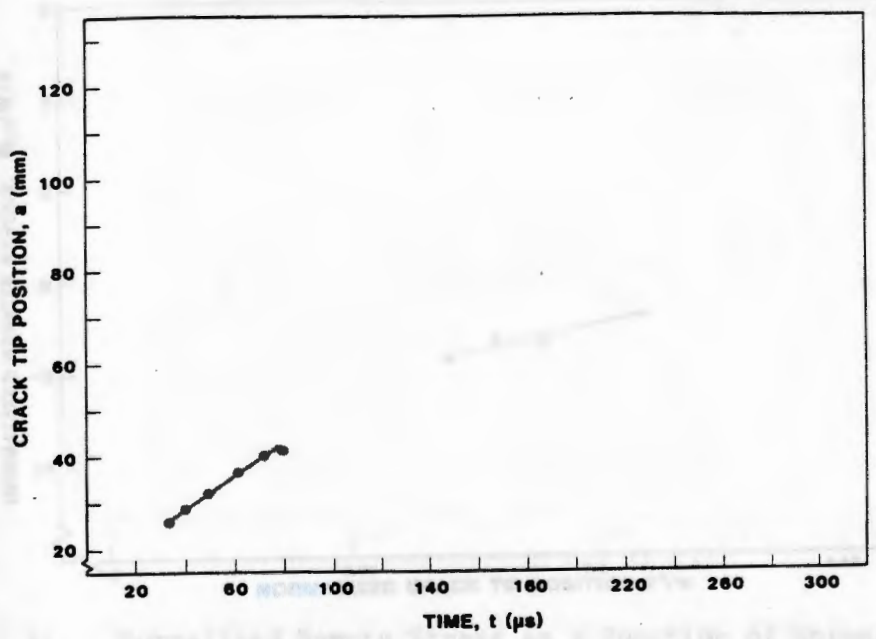


FIG. 29. Crack Extension vs. Time Plot for Experiment 7.

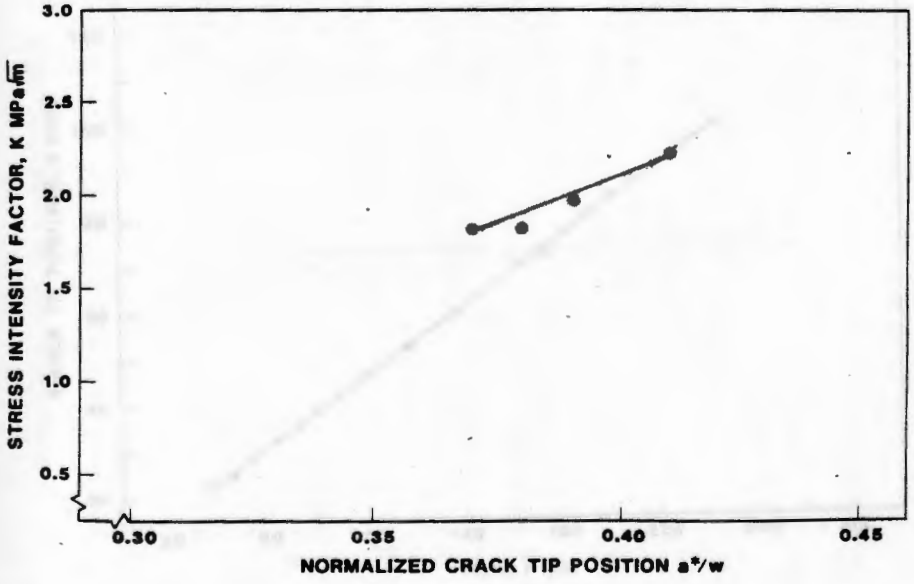


FIG. 30. Stress Intensity Factor as a Function of Normalized Crack Tip Position for Experiment 7.

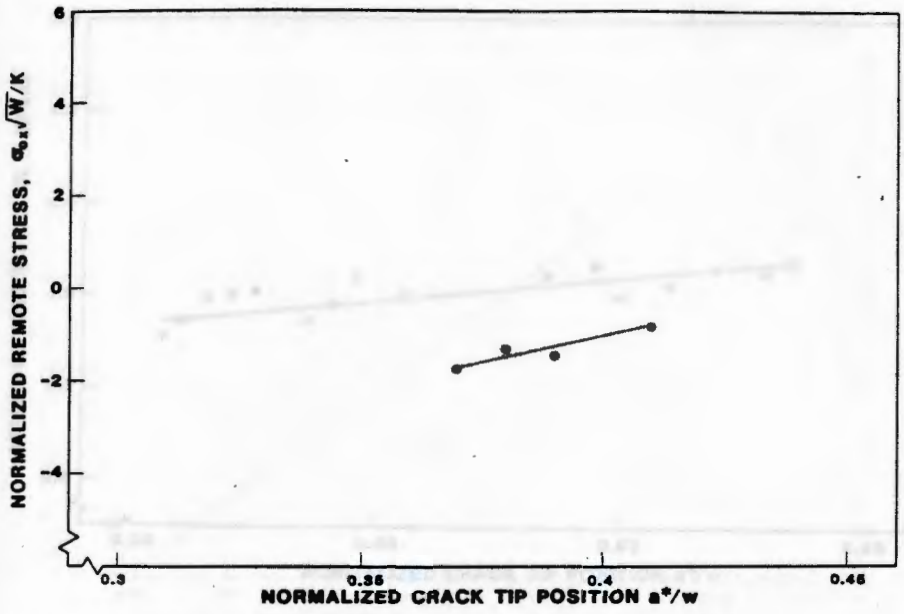


FIG. 31. Normalized Remote Stress as a Function of Normalized Crack Tip Position for Experiment 7.

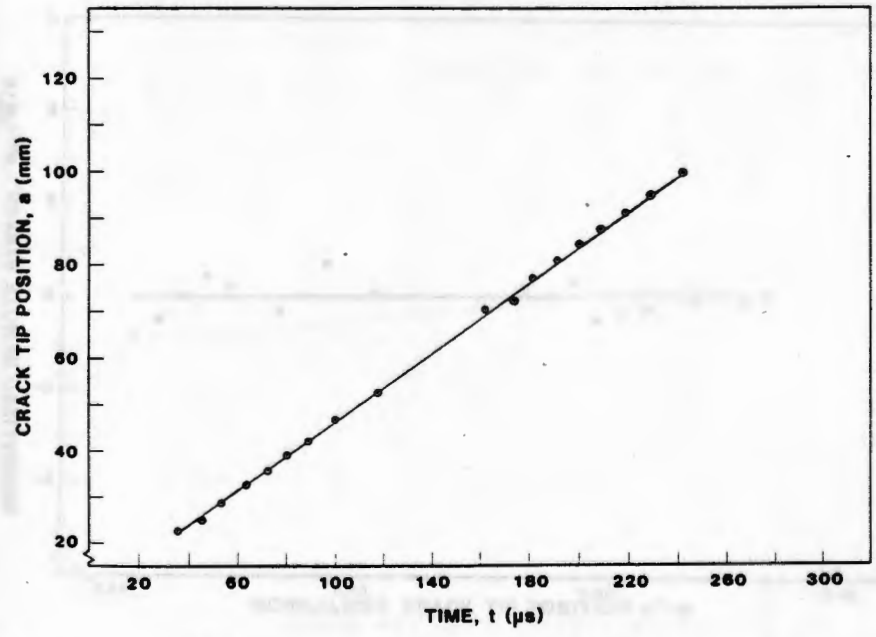


FIG. 32. Crack Extension vs. Time Plot for Experiment 8.

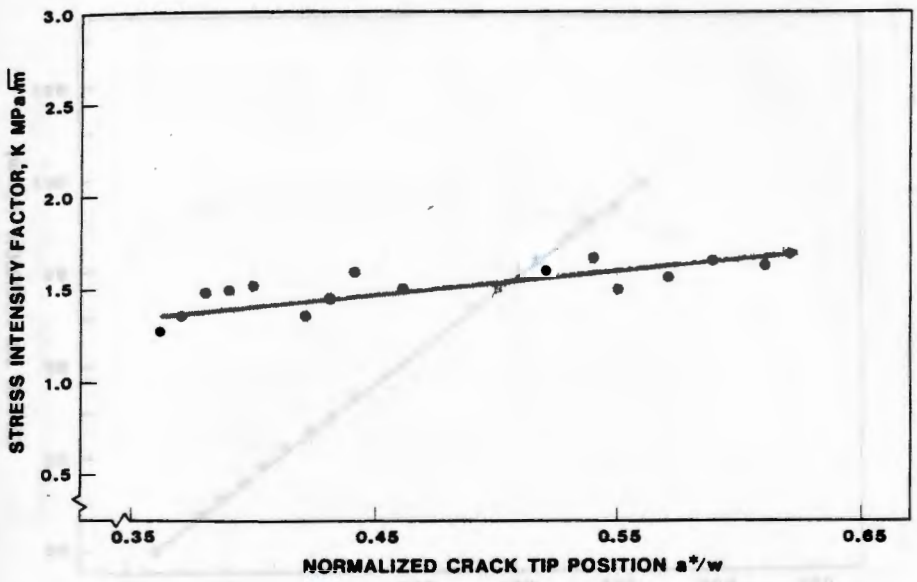


FIG. 33. Stress Intensity Factor as a Function of Normalized Crack Tip Position for Experiment 8.

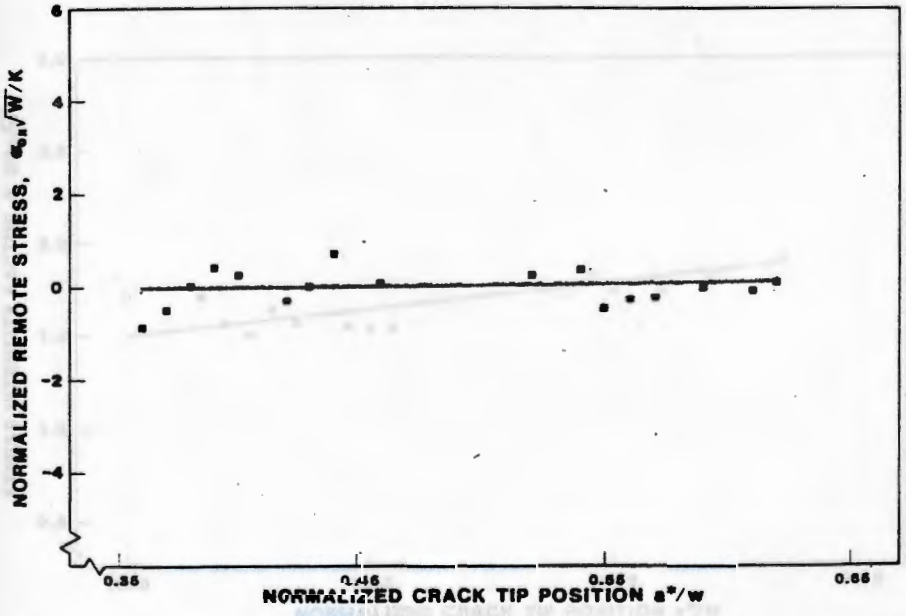


FIG. 34. Normalized Remote Stress as a Function of Normalized Crack Tip Position for Experiment 8.

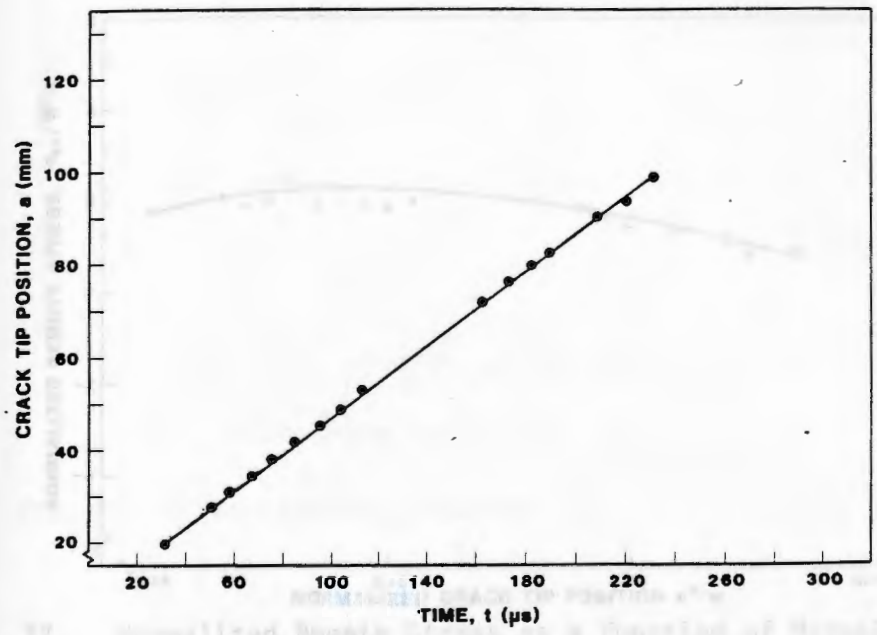


FIG. 35. Crack Extension vs. Time Plot for Experiment 9.

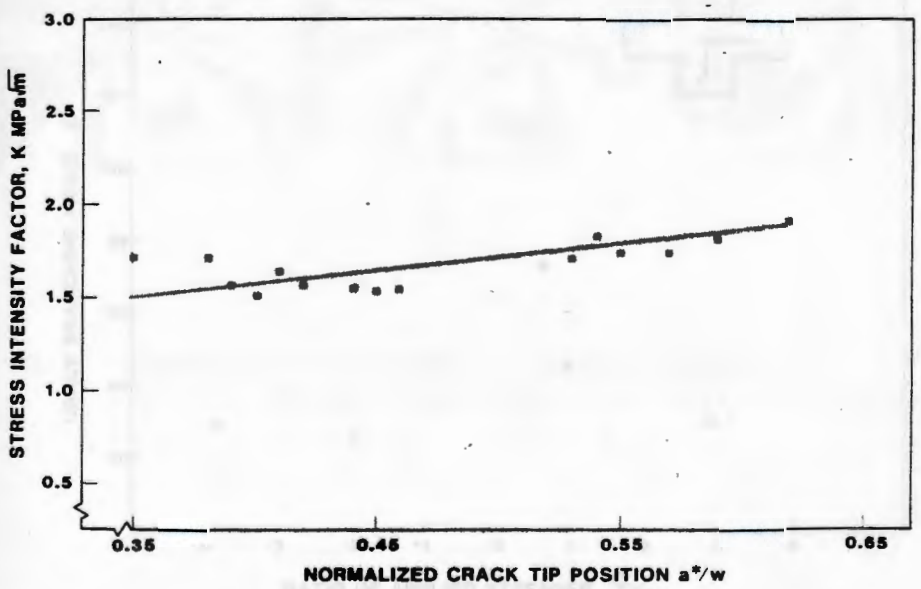


FIG. 36. Stress Intensity Factor as a Function of Normalized Crack Tip Position for Experiment 9.

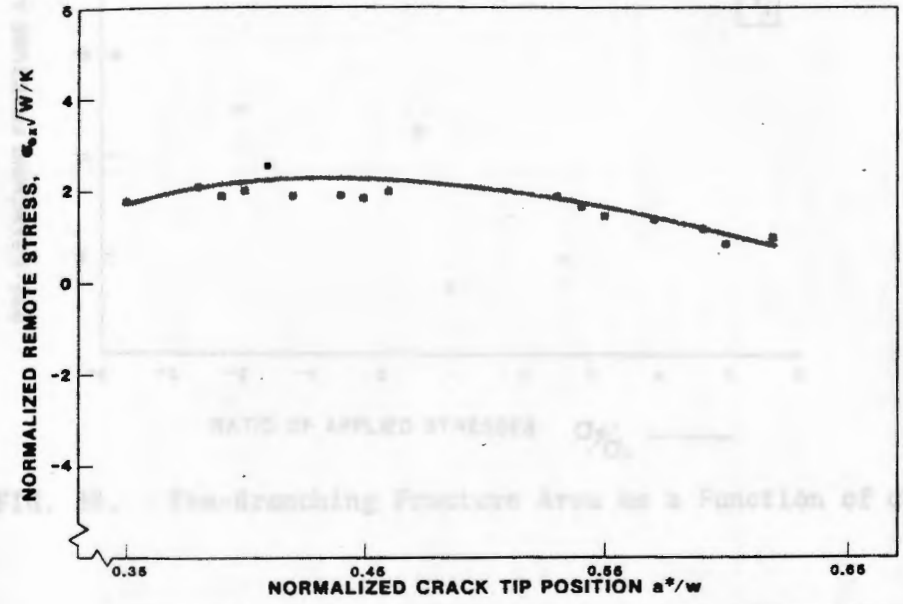


FIG. 37. Normalized Remote Stress as a Function of Normalized Crack Tip Position for Experiment 9.

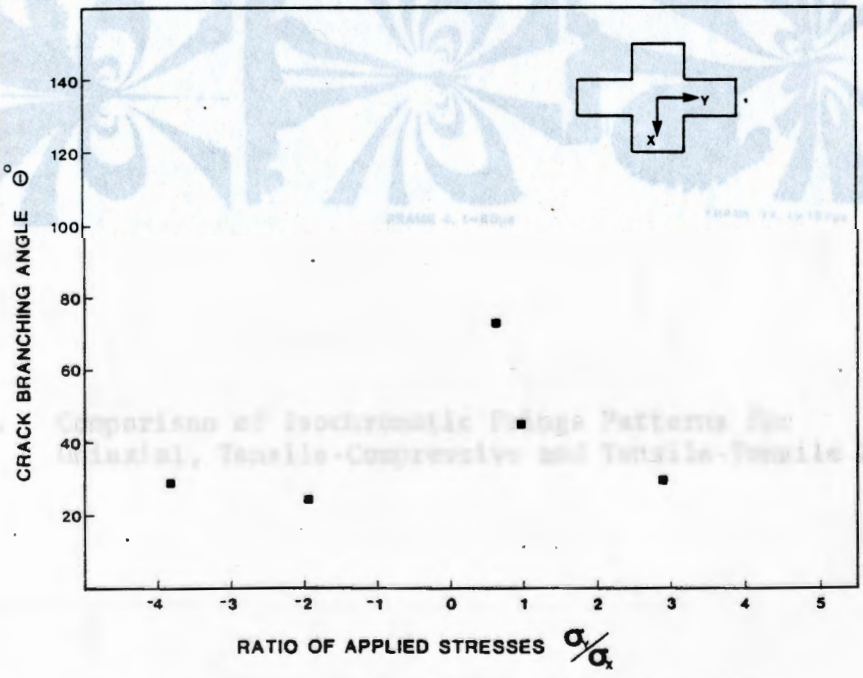


FIG. 38. $\sigma_y/\sigma_x$ as a Function of Branching Angle.

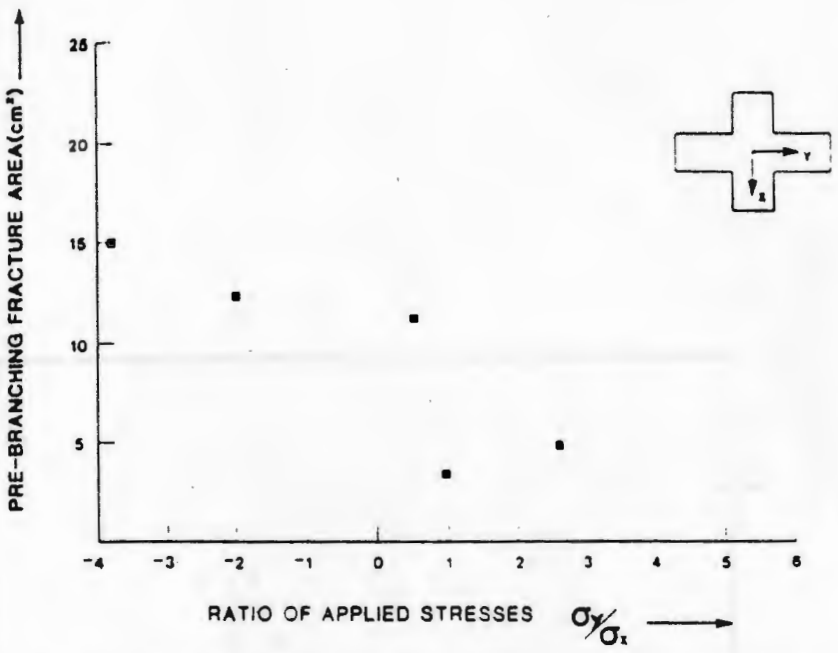


FIG. 39. Pre-Branching Fracture Area as a Function of $\sigma_y/\sigma_x$.

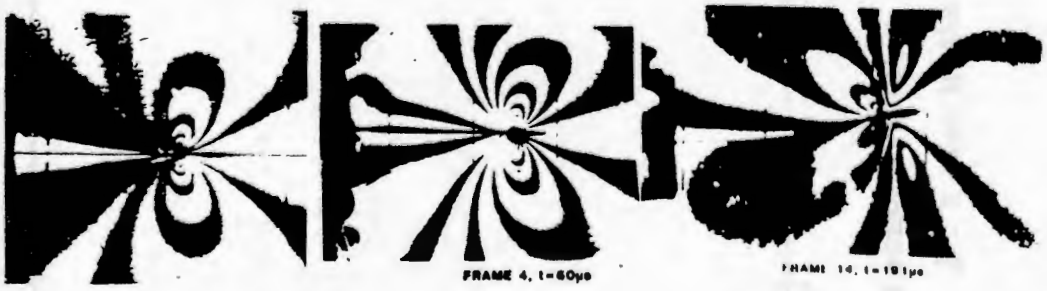


FIG. 40. Comparison of Isochromatic Fringe Patterns for Uniaxial, Tensile-Compressive and Tensile-Tensile Loading.

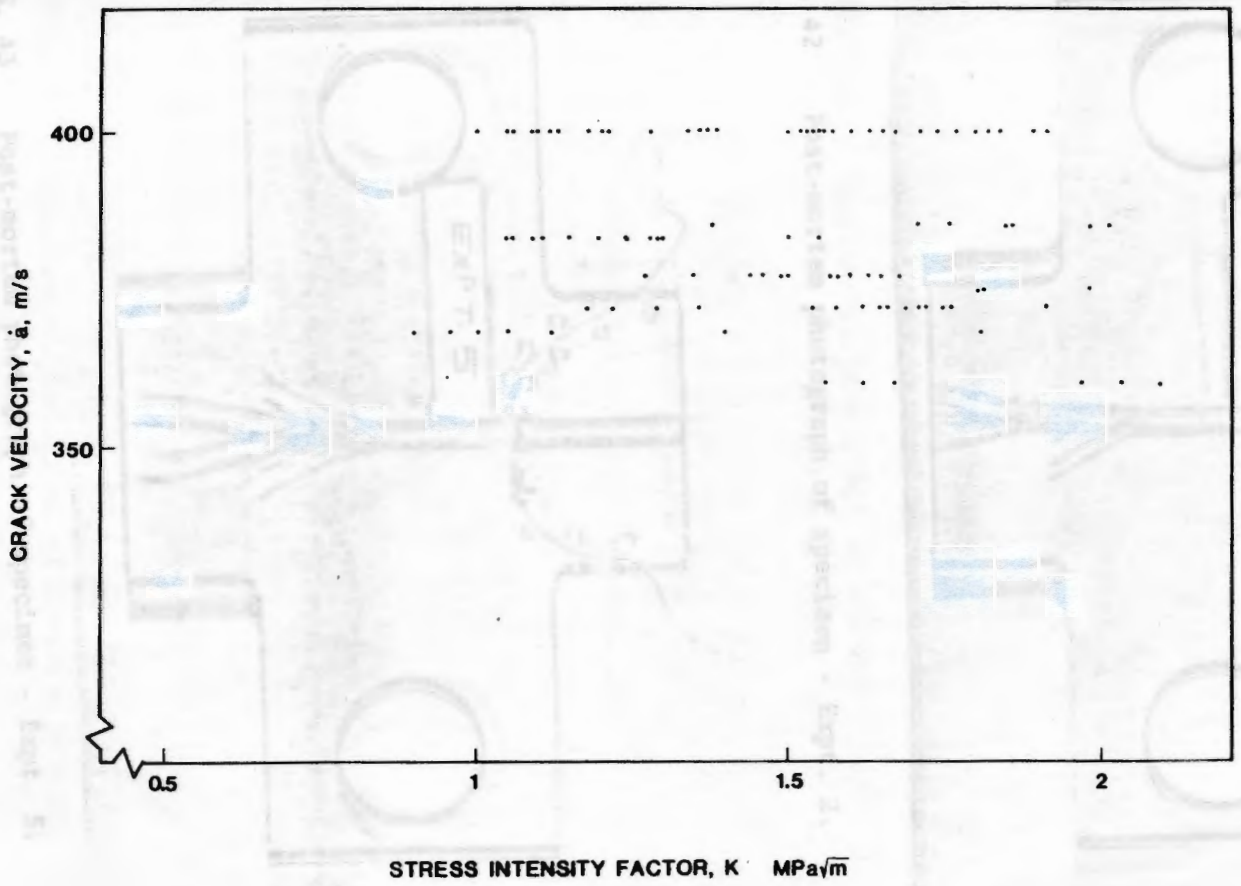


FIG. 41. $\dot{a}$ - K Plot in the High Velocity Region.

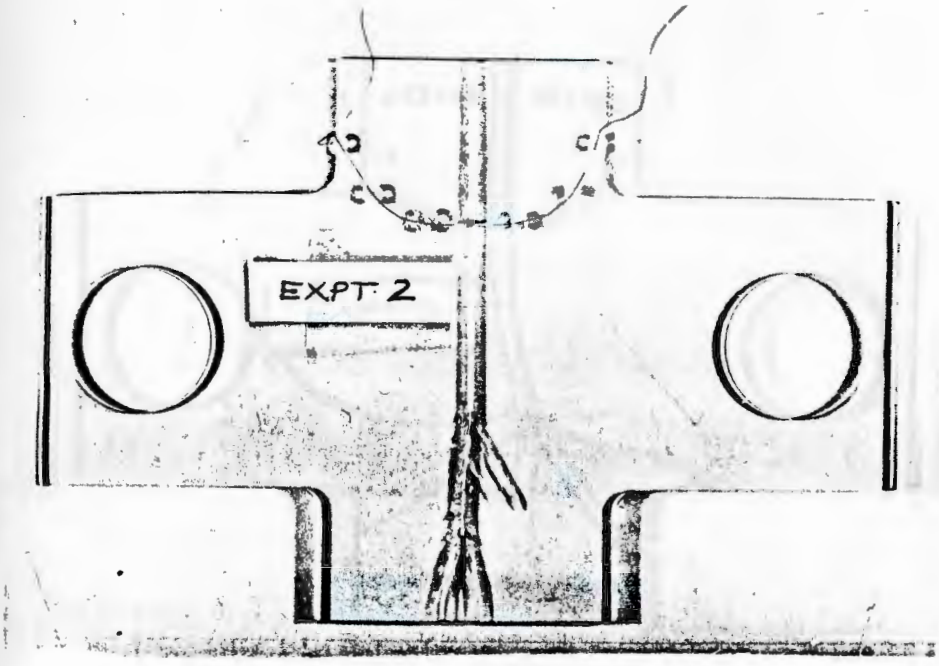


FIG. 42 Post-mortem photograph of specimen - Expt. 2.

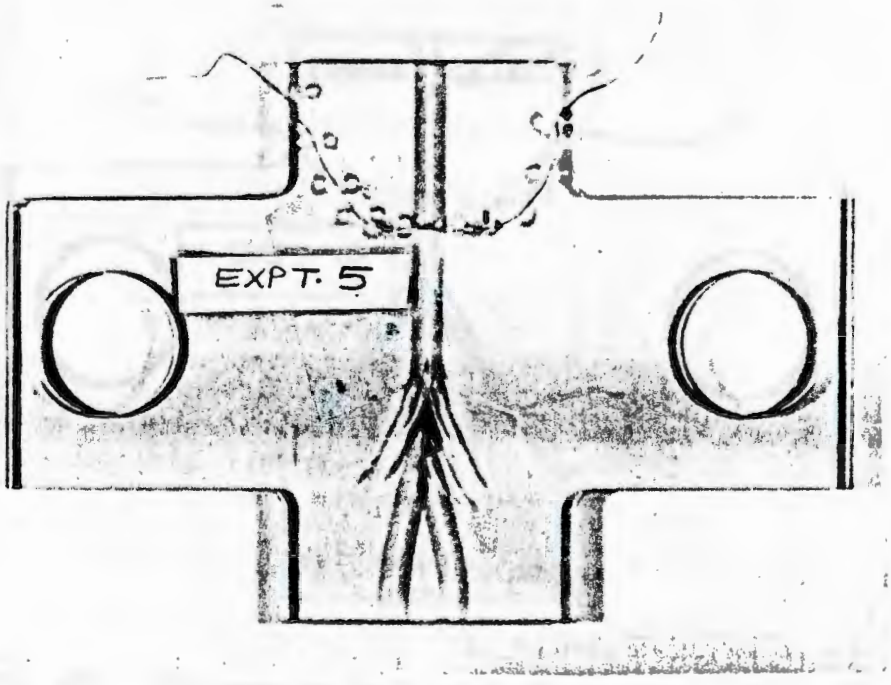


FIG. 43 Post-mortem photograph of specimen - Expt. 5.

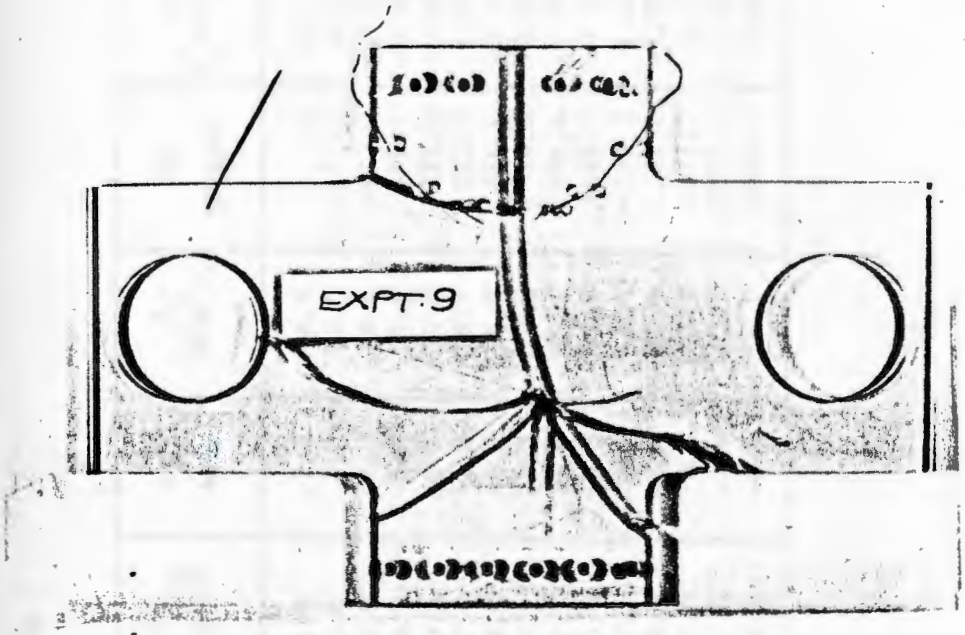


FIG. 44 Post-mortem photograph of specimen - Expt. 9.

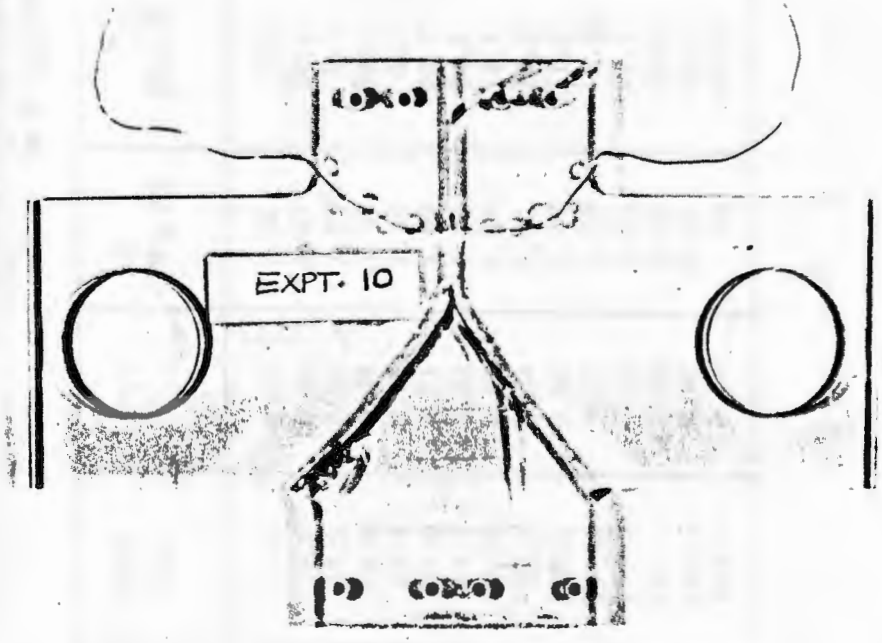


FIG. 45. Post-mortem photograph of specimen - Expt. 10.

TABLE 1

OUTPUT VALUES FOR EXPT. NO. 1

($\dot{a}$ = 383 m/s)

| FRAME NO. | TIME (μs) | a*/w | K MPa $\sqrt{m}$ | $A_1$ MPa/$\sqrt{m}$ | $A_2$ MPa/$m^{1.5}$ | $\sigma_{ox}$ MPa | $B_1$ MPa/m | $B_2$ MPa/$m^2$ | $B'_o = \frac{\sigma_{ox}\sqrt{w}}{K}$ |
|---|---|---|---|---|---|---|---|---|---|
| 1 | 13.0 | 0.44 | 1.06 | -2.8 | -71.9 | -2.3 | 4.8 | 7.9 | -1.17 |
| 3 | 30.0 | 0.46 | 1.47 | -37.6 | 43.6 | 1.4 | 20.6 | -683.0 | 0.52 |
| 4 | 39.5 | 0.47 | 1.15 | 0.9 | 109.6 | -2.2 | -8.8 | -477.0 | -1.03 |
| 5 | 49.0 | 0.48 | 1.09 | -29.5 | -653.0 | -1.8 | 58.4 | 545.0 | -0.89 |
| 6 | 57.5 | 0.49 | 1.24 | 8.2 | 339.5 | -2.1 | -28.7 | -732.0 | -0.92 |
| 7 | 67.5 | 0.51 | 1.00 | -28.7 | -977.0 | -2.6 | 78.1 | 1322.0 | -1.41 |
| 8 | 77.5 | 0.52 | 1.28 | -34.6 | -518.0 | -0.7 | 55.4 | 456.0 | -0.30 |
| 9 | 86.5 | 0.53 | 1.29 | -14.4 | -52.2 | -1.3 | 9.6 | -4.9 | -0.55 |
| 10 | 95.0 | 0.54 | 1.11 | -18.2 | -541.7 | -2.6 | 39.1 | 606.0 | -1.27 |
| 11 | 139.5 | 0.60 | 1.40 | -51.5 | -996.0 | -0.5 | 99.9 | 1155.0 | -0.19 |
| 12 | 151.5 | 0.62 | 1.30 | -0.84 | 29.1 | -2.7 | -8.6 | -112.0 | -1.12 |
| 14 | 171.5 | 0.64 | 1.05 | -21.9 | -878.0 | -3.8 | 61.6 | 1191.0 | -1.96 |
| 15 | 181.0 | 0.66 | 1.55 | -59.4 | -963.0 | 0.4 | 104.0 | 1074.0 | 0.14 |
| 16 | 190.5 | 0.67 | 1.11 | -21.1 | -1156.0 | -4.0 | 82.7 | 1857.0 | -1.95 |
| 17 | 203.5 | 0.68 | .99 | -22.9 | -1469.0 | -4.8 | 97.0 | 2459.0 | -2.62 |

TABLE 2

OUTPUT VALUES FOR EXPT. NO. 2

($\dot{a}$ = 400 m/s)

| FRAME NO. | TIME (μs) | a*/w | K MPa $\sqrt{m}$ | $A_1$ MPa/$\sqrt{m}$ | $A_2$ MPa/$m^{1.5}$ | $\sigma_{ox}$ MPa | $B_1$ MPa/m | $B_2$ MPa/$m^2$ | $B_o' := \frac{\sigma_{ox}\sqrt{w}}{K}$ |
|---|---|---|---|---|---|---|---|---|---|
| 1 | 15.0 | 0.33 | 1.12 | -17.5 | -253 | -1.6 | 14.4 | 33 | -0.77 |
| 2 | 26.0 | 0.34 | 1.09 | -10.7 | -430 | -2.4 | 18.6 | 616 | -1.19 |
| 3 | 37.5 | 0.35 | 1.13 | -10.3 | -557 | -2.6 | 28.5 | 884 | -1.24 |
| 4 | 44.5 | 0.37 | 1.21 | 18.3 | 27 | -2.6 | -19.2 | 469 | -1.16 |
| 5 | 53.0 | 0.38 | 1.37 | -45.0 | -930 | -0.3 | 83.4 | 1194 | -0.12 |
| 6 | 63.5 | 0.39 | 1.28 | 0.2 | -99 | -2.4 | -3.0 | 172 | -1.01 |
| 8 | 83.5 | 0.42 | 1.37 | 6.8 | 87 | -2.2 | -11.4 | -126 | -0.87 |
| 9 | 93.5 | 0.43 | 1.65 | -39.5 | -329 | 1.0 | 50.0 | 405 | 0.33 |
| 10 | 103.0 | 0.45 | 1.63 | -42.0 | -472 | 0.6 | 59.0 | 509 | 0.20 |
| 11 | 139.5 | 0.50 | 1.77 | -49.0 | -648 | 0.4 | 78.0 | 560 | 0.12 |
| 12 | 145.0 | 0.51 | 1.80 | -30.0 | -278 | -0.4 | 35.0 | 71 | -0.12 |
| 14 | 167.5 | 0.54 | 1.89 | -38.0 | -438 | -0.1 | 54.0 | 343 | -0.03 |
| 15 | 174.0 | 0.55 | 1.67 | -22.0 | -706 | -2.9 | 53.0 | 966 | -0.94 |
| 16 | 183.0 | 0.56 | 1.73 | -10.8 | -333 | -2.9 | 23.0 | 389 | -0.91 |
| 17 | 193.5 | 0.58 | 1.80 | -13.4 | -365 | -3.0 | 23.0 | 374 | -0.90 |
| 19 | 223.5 | 0.62 | 1.84 | -21.0 | -478 | -3.3 | 41.0 | 444 | -0.97 |

TABLE 3

OUTPUT VALUES FOR EXPT. NO. 3

($\dot{a}$ = 368 m/s)

| FRAME NO. | TIME (μs) | a*/w | K MPa $\sqrt{m}$ | $A_1$ MPa/$\sqrt{m}$ | $A_2$ MPa/$m^{1.5}$ | $\sigma_{ox}$ MPa | $B_1$ MPa/m | $B_2$ MPa/$m^2$ | $B_o' = \frac{\sigma_{ox}\sqrt{w}}{K}$ |
|---|---|---|---|---|---|---|---|---|---|
| 1 | 13.5 | 0.39 | 0.90 | 8.6 | 250 | -2.6 | -27.0 | -74 | -0.78 |
| 3 | 30.5 | 0.40 | 0.96 | -2.7 | -285 | -2.4 | 11.0 | 577 | -0.68 |
| 4 | 40.5 | 0.42 | 1.00 | -21.2 | -400 | -1.8 | 31.0 | 377 | -0.46 |
| 6 | 57.5 | 0.44 | 0.96 | 17.7 | -507 | -3.4 | 20.0 | 1558 | -0.97 |
| 7 | 66.5 | 0.45 | 1.12 | 4.6 | -331 | -2.2 | 11.0 | 1039 | -0.55 |
| 9 | 85.0 | 0.48 | 1.05 | 13.2 | -281 | -3.2 | 10.0 | 769 | -0.82 |
| 12 | 152.5 | 0.56 | 1.40 | -11.6 | 60 | -1.4 | -4.0 | -176 | -0.26 |
| 15 | 179.0 | 0.59 | 1.81 | -13.2 | 460 | 0.4 | -40.0 | -602 | 0.07 |

TABLE 4

OUTPUT VALUES FOR EXPT. NO. 4

($\dot{a}$ = 400 m/s)

| FRAME NO. | TIME (μs) | a*/w | K MPa $\sqrt{m}$ | $A_1$ MPa/$\sqrt{m}$ | $A_2$ MPa/$m^{1.5}$ | $\sigma_{ox}$ MPa | $B_1$ MPa/m | $B_2$ MPa/$m^2$ | $B_o' = \frac{\sigma_{ox}\sqrt{w}}{K}$ |
|---|---|---|---|---|---|---|---|---|---|
| 1 | 31.0 | 0.37 | 0.98 | -25 | -706 | -2.2 | 47 | 983 | -1.21 |
| 2 | 39.0 | 0.38 | 1.18 | -4 | 330 | -1.4 | 0 | -862 | -0.64 |
| 4 | 57.5 | 0.41 | 1.12 | -15 | -376 | -2.0 | 28 | 593 | -0.97 |
| 5 | 66.0 | 0.42 | 1.10 | -19 | -519 | -2.2 | 39 | 742 | -1.10 |
| 6 | 75.5 | 0.43 | 1.20 | -16 | -42 | -1.6 | 9 | -77 | -0.72 |
| 7 | 84.0 | 0.44 | 1.06 | -20 | -599 | -3.0 | 40 | 786 | -1.53 |
| 9 | 103.5 | 0.47 | 1.34 | -11 | -206 | -1.8 | 5 | 649 | -0.73 |
| 10 | 113.5 | 0.48 | 1.05 | -86 | -2523 | -2.2 | 146 | 2727 | -1.13 |
| 11 | 142.5 | 0.51 | 1.03 | -27 | -2066 | -5.0 | 94 | 4486 | -2.62 |
| 12 | 153.0 | 0.53 | 1.39 | -32 | -720 | -2.4 | 34 | 1057 | -0.93 |
| 14 | 171.5 | 0.55 | 1.36 | -35 | -1169 | -2.8 | 81 | 1908 | -1.11 |
| 15 | 180.5 | 0.57 | 1.57 | -36 | -935 | -1.8 | 63 | 1572 | -0.62 |
| 16 | 190.5 | 0.58 | 2.46 | -75 | 434 | 5.2 | 13 | 316 | 1.14 |
| 17 | 201.5 | 0.60 | 2.47 | -73 | -758 | 4.4 | 92 | 1941 | 0.96 |
| 19 | 226.0 | 0.63 | 1.77 | -64 | -1229 | -0.4 | 92 | 1589 | -0.12 |

TABLE 5

OUTPUT VALUES FOR EXPT. NO. 5

($\dot{a}$ = 385 m/s)

| FRAME NO. | TIME (μs) | a*/w | K MPa $\sqrt{m}$ | $A_1$ MPa/$\sqrt{m}$ | $A_2$ MPa/$m^{1.5}$ | $\sigma_{ox}$ MPa | $B_1$ MPa/m | $B_2$ MPa/$m^2$ | $B'_o = \frac{\sigma_{ox}\sqrt{w}}{K}$ |
|---|---|---|---|---|---|---|---|---|---|
| 1 | 33.5 | 0.44 | 1.86 | -74.4 | -1193 | -0.6 | 117 | 1155 | -0.17 |
| 2 | 41.5 | 0.45 | 1.76 | -7.1 | 443 | -3.8 | -38 | -1516 | -1.17 |
| 3 | 50.0 | 0.46 | 1.71 | -18.8 | -330 | -4.2 | 22 | 165 | -1.33 |
| 4 | 60.0 | 0.48 | 1.38 | 40.5 | -2028 | -8.6 | 102 | 6617 | -3.37 |
| 5 | 69.0 | 0.49 | 1.85 | -93.4 | -2715 | -2.4 | 173 | 3869 | -0.70 |
| 7 | 87.5 | 0.51 | 1.98 | -22.2 | -240 | -3.4 | 19 | 11 | -0.93 |
| 8 | 98.0 | 0.53 | 2.01 | -100.9 | -3696 | -2.8 | 266 | 5333 | -0.75 |

TABLE 6

OUTPUT VALUES FOR EXPT. NO. 6

($\dot{a}$ = 372 m/s)

| FRAME NO. | TIME (μs) | a*/w | K MPa $\sqrt{m}$ | $A_1$ MPa/$\sqrt{m}$ | $\sigma_{ox}$ MPa | $B_1$ MPa/m | $k'_o = \frac{\sigma_{ox}\sqrt{w}}{K}$ |
|---|---|---|---|---|---|---|---|
| 1 | 34.5 | 0.38 | 1.18 | 9.0 | -6.8 | -17 | -3.11 |
| 2 | 43.0 | 0.39 | 1.22 | 6.7 | -6.6 | -20 | -2.92 |
| 3 | 51.0 | 0.40 | 1.29 | 8.2 | -6.5 | -16 | -2.72 |
| 4 | 61.0 | 0.42 | 1.36 | 7.3 | -6.3 | -15 | -2.50 |
| 7 | 88.5 | 0.45 | 1.54 | 1.4 | -5.4 | -18 | -1.90 |
| 8 | 97.5 | 0.46 | 1.58 | 2.0 | -5.5 | -17 | -1.88 |
| 9 | 106.5 | 0.47 | 1.62 | 6.0 | -6.4 | -25 | -2.14 |
| 10 | 116.0 | 0.48 | 1.58 | 4.0 | -6.2 | -15 | -2.12 |
| 11 | 120.5 | 0.49 | 1.69 | 1.6 | -5.4 | -22 | -1.73 |
| 12 | 131.0 | 0.50 | 1.72 | -1.6 | -5.4 | -15 | -1.70 |
| 14 | 148.0 | 0.53 | 1.66 | 4.8 | -7.4 | -20 | -2.41 |
| 15 | 156.5 | 0.54 | 1.65 | 7.8 | -8.4 | -15 | -2.75 |
| 16 | 166.0 | 0.55 | 1.76 | 8.9 | -8.4 | -26 | -2.58 |
| 17 | 176.0 | 0.57 | 1.71 | 6.5 | -8.4 | -23 | -2.66 |
| 18 | 185.5 | 0.58 | 1.91 | 6.4 | -7.4 | -30 | -2.09 |
| 19 | 197.5 | 0.59 | 1.75 | 14.0 | -9.8 | -23 | -3.03 |

TABLE 7

OUTPUT VALUES FOR EXPT. NO. 7

($\dot{a}$ = 375 m/s)

| FRAME NO. | TIME (μs) | a*/w | K MPa $\sqrt{m}$ | $A_1$ MPa/$\sqrt{m}$ | $A_2$ MPa/$m^{1.5}$ | $\sigma_{ox}$ MPa | $B_1$ MPa/m | $B_2$ MPa/$m^2$ | $B_o' = \frac{\sigma_{ox}\sqrt{w}}{K}$ |
|---|---|---|---|---|---|---|---|---|---|
| 1 | 32.5 | 0.37 | 1.81 | 46 | -610 | -6.0 | 8 | 1568 | -1.79 |
| 2 | 40.0 | 0.38 | 1.82 | -27 | -1195 | -4.4 | 86 | 960 | -1.31 |
| 3 | 49.5 | 0.39 | 1.98 | 48 | 397 | -5.4 | -58 | -696 | -1.47 |
| 4 | 60.0 | 0.41 | 2.21 | 27 | 171 | -3.4 | -34 | 134 | -0.83 |

TABLE 8

OUTPUT VALUES FOR EXPT. NO. 8

($\dot{a}$ = 377 m/s)

| FRAME NO. | TIME (μs) | a*/w | K MPa $\sqrt{m}$ | $A_1$ MPa/$\sqrt{m}$ | $A_2$ MPa/$m^{1.5}$ | $\sigma_{ox}$ MPa | $B_1$ MPa/m | $B_2$ MPa/$m^2$ | $B_o' = \frac{\sigma_{ox}\sqrt{w}}{K}$ |
|---|---|---|---|---|---|---|---|---|---|
| 1 | 35.5 | 0.36 | 1.27 | 50.9 | 102 | -2.0 | -84 | 94 | -0.85 |
| 2 | 46.0 | 0.37 | 1.35 | 45.1 | 237 | -1.2 | -78 | 704 | -0.48 |
| 3 | 52.0 | 0.38 | 1.46 | 24.8 | 926 | 0 | -101 | -1933 | 0 |
| 4 | 62.5 | 0.39 | 1.49 | -31.2 | -1346 | 1.0 | 104 | 2807 | 0.36 |
| 5 | 71.5 | 0.40 | 1.50 | 18.7 | 1146 | 0.6 | -87 | -2277 | 0.22 |
| 6 | 79.5 | 0.42 | 1.35 | 52.4 | 943 | -0.8 | -108 | -541 | -0.32 |
| 7 | 89.0 | 0.43 | 1.44 | 28.7 | 867 | 0 | -81 | -1396 | 0 |
| 8 | 99.5 | 0.44 | 1.58 | -14.0 | 642 | 2.0 | -21 | -1663 | 0.68 |
| 10 | 117.5 | 0.46 | 1.50 | 23.3 | 849 | 0.2 | -74 | -1710 | 0.07 |
| 11 | 162.0 | 0.52 | 1.60 | 26.7 | 359 | 0.6 | -46 | 310 | 0.20 |
| 12 | 173.5 | 0.54 | 1.65 | 20.7 | 544 | 1.0 | -51 | -483 | 0.33 |
| 13 | 181.0 | 0.55 | 1.50 | 44.0 | 219 | -1.2 | -59 | 142 | -0.43 |
| 14 | 191.5 | 0.56 | 1.55 | 39.1 | 248 | -0.6 | -60 | 262 | -0.21 |
| 15 | 199.5 | 0.57 | 1.57 | 36.2 | 250 | -0.6 | -58 | 147 | -0.21 |
| 17 | 219.0 | 0.59 | 1.65 | 29.5 | 594 | -0.2 | -71 | -695 | -0.07 |
| 18 | 228.5 | 0.61 | 1.63 | 34.1 | 437 | -0.4 | -62 | -523 | -0.13 |
| 19 | 241.5 | 0.62 | 1.68 | 13.1 | 481 | 0.3 | -34 | -1167 | 0.08 |

TABLE 9

OUTPUT VALUES FOR EXPT. NO. 9

($\dot{a}$ = 400 m/s)

| FRAME NO. | TIME (μs) | a*/w | K MPa $\sqrt{m}$ | $A_1$ MPa/$\sqrt{m}$ | $A_2$ MPa/$m^{1.5}$ | $\sigma_{ox}$ MPa | $B_1$ MPa/m | $B_2$ MPa/$m^2$ | $k'_o = \frac{\sigma_{ox}\sqrt{w}}{K}$ |
|---|---|---|---|---|---|---|---|---|---|
| 1 | 31.0 | 0.35 | 1.52 | 5.1 | -401 | 5.0 | 31.1 | 1874 | 1.78 |
| 3 | 50.0 | 0.38 | 1.60 | -8.4 | 77 | 6.1 | 1.0 | 151 | 2.06 |
| 4 | 58.0 | 0.39 | 1.56 | -2.5 | -216 | 5.6 | 10.7 | 690 | 1.94 |
| 5 | 67.0 | 0.40 | 1.50 | 0.6 | 26 | 5.8 | 9.3 | 724 | 2.09 |
| 6 | 76.0 | 0.41 | 1.64 | -35.0 | 1167 | 7.6 | 1.4 | -2958 | 2.51 |
| 7 | 85.0 | 0.42 | 1.57 | 3.2 | -252 | 5.6 | 13.5 | 1248 | 1.93 |
| 8 | 95.5 | 0.44 | 1.55 | 2.8 | -325 | 5.6 | 18.0 | 1167 | 1.95 |
| 9 | 103.5 | 0.45 | 1.53 | 5.3 | -387 | 5.4 | 30.5 | 1737 | 1.91 |
| 10 | 113.0 | 0.46 | 1.54 | -0.6 | -275 | 5.8 | 18.6 | 897 | 2.04 |
| 11 | 162.5 | 0.53 | 1.71 | -3.8 | 87 | 5.8 | -5.7 | -1195 | 1.83 |
| 12 | 173.0 | 0.54 | 1.83 | -5.1 | -237 | 5.6 | -1.8 | 342 | 1.65 |
| 13 | 181.5 | 0.55 | 1.73 | 4.4 | -910 | 4.6 | 47.6 | 2265 | 1.44 |
| 14 | 191.0 | 0.57 | 1.74 | 11.5 | -143 | 4.4 | -7.6 | 683 | 1.37 |
| 16 | 209.5 | 0.59 | 1.82 | 9.5 | 486 | 3.8 | -48.4 | -1000 | 1.13 |
| 17 | 220.0 | 0.60 | 1.82 | 21.2 | -3 | 2.8 | -32.8 | 1032 | 0.83 |
| 18 | 231.5 | 0.62 | 1.91 | 13.3 | -379 | 3.4 | -6.5 | 1851 | 0.96 |

TABLE 10

$K_{br}$, Branching Angles and Pre-branching Fracture Areas for all the Experiments

| EXPT. NO. | $\sigma_y$ (MPA) | $\sigma_x$ (MPA) | Pre-branching fracture area $(cm)^2$ | Branching Angle (degrees) | $K_{br}$ (MPA $\sqrt{m}$ |
|---|---|---|---|---|---|
| #2 | 3.85 | 0 | 17.8 | 23 | 1.84 (branching attempt) |
| #5 | 4.6 | -1.2 | 15.0 | 29 | 2.01 |
| #6 | 4.6 | -2.34 | 12.4 | 24.5 | 1.91 |
| #7 | 4.75 | 1.65 | 4.8 | 30 | 2.2 |
| #9 | 3.71 | 6.4 | 10.8 | 73 | 1.91 |
| #10 | 4.51 | 4.66 | 3.5 | 45° | 2 |

TABLE 11

Summary of Calculated $r_o$ Values

| EXPT. NO. | $K_{br}$ (MPA$\sqrt{m}$) | $\sigma_{ox}$ (MPA) | $r_o$ (MM) |
|---|---|---|---|
| 5 | 2.01 | -2.8 | 8.1 |
| 6 | 1.91 | -7.4 | 1.1 |
| 7 | 2.21 | -3.4 | 6.8 |
| 9 | 1.91 | 3.4 | 4.8 |

# APPENDIX

```
10      DISP "HELLO,  PLEASE SEE CRT OR PRINTER FOR INSTRUCTIONS"
20      WAIT 3000
30      DISP "THIS PROGRAM USES DYN.6 PARA-MODEL : ALL OUTPUT IN S.I.UNITS"
40      WAIT 3000
50      DISP "DATA TO BE FED THRU DIGITIZER INCLUDING FR.ORDER"
60      WAIT 3000
70      DISP "IF THE VALUES CONVERGE BEFORE ASSIGNED ITRNS. STOP PROGRAM"
80      WAIT 3000
90      DISP " NOW YOU MAY START"
100     WAIT 2000
110     PRINT "FEED EXPT & FRAME NO."
120     INPUT O2,O3
130     PRINTER IS 0
140     PRINT USING "K";"EXPT",O2," ","FRAME",O3
150     PRINT "----- --------"
160     PRINTER IS 16
170     PRINT "FEED IN INITIAL A0 ETC.-ALL IN S.I. UNITS"
180     INPUT A0,A1,A2,B0,B1,B2
190     PRINT "INITIAL A0 ETC.=",A0,A1,A2,B0,B1,B2
200     PRINT "FEED IN C,C1,C2-ALL IN M/SEC"
210     INPUT C,C1,C2
220     PRINT "C=",C,"C1=",C1,"C2=",C2
230     PRINT "FEED IN FSIGMA(F) IN MPA-M/FRINGE & THICKNESS(H) IN METER"
240     INPUT F,H
250     PRINT "FSIGMA=",F,"THICKNESS=",H
260     PRINT "FEED IN MINIMUM FRINGE ORDER TAKEN,N100"
270     INPUT N100
280     PRINT "N-MINIMUM=",N100
290     DISP "DO YOU WANT INSTRUCTNS. FOR FEEDING FR.ORDERS ON THERMAL PRINTER?"
300     WAIT 3000
310     DISP "IF YES, FEED I=1; IF NO, FEED I=0"
320     WAIT 3000
330     INPUT "FEED I",I
340     IF I=0 THEN PRINTER IS 16
350     IF I=1 THEN PRINTER IS 0
360     PRINT USING "K";"FR.ORDER","    ","BUTTON ORDER"
370     FOR J=0 TO 6
380     PRINT USING 390;N100+.5*J,J
390     IMAGE 2X,D.D,10X,D
400     NEXT J
410     PRINTER IS 16
420     DIM R(60),O(60),N(60),G(60),A(60,6),U(6,60),Q(6,6),W(6,6),Y(6,6),P(6),X(6
),X1(60),Y1(60),C(60),N1(60),N2(60),D(60),T(60)
430     PRINT "FEED TOTAL NO. OF DATA PTS."
440     INPUT N3
450     PRINT "INPUT ACTUAL DISTANCE BETWEEN 2 ADJACENT MARKS(D) IN INCHES"
460     INPUT D
470     PRINT "TO FIND SCALE FACTOR,INPUT CO-ORDINATES OF MARKS(X1,Y1,X2,Y2)"
480     ENTER 701;S5,X1,Y1
490     ENTER 701;S5,X2,Y2
500     PRINT X1,Y1,X2,Y2
510     R1=SQR((Y2-Y1)^2+(X2-X1)^2)
520     M0=D/R1
530     PRINT "SCALE FACTOR=",M0
540     PRINT "TO FIND INCLINATION OF CRACK LINE,FEED CO-ORDINATES OF 2 PTS.ON CR
ACK LINE(X3,Y3,X4,Y4)"
550     ENTER 701;S5,X3,Y3
560     ENTER 701;S5,X4,Y4
570     Y7=Y4-Y3
580     X7=X4-X3
590     O1=ATN(Y7/X7)
600     IF (Y7>=0) AND (X7>=0) THEN O1=O1
610     IF (Y7>=0) AND (X7<0) THEN O1=O1+PI
620     IF (Y7<0) AND (X7<0) THEN O1=O1-PI
630     IF (Y7<0) AND (X7>0) THEN O1=O1

640     A3=O1*180/PI
650     PRINT "INCLINATION OF CRACK LINE(IN DEG.)=",A3
660     PRINT "FEED CRACK TIP LOCATION (X5,Y5)"
670     ENTER 701;S5,X5,Y5
680     PRINT "CRACK TIP CO-ORDINATES ARE AS FOLLOWS;-"
690     PRINT X5,Y5
691     PRINTER IS 0
700     PRINT USING "X,K,14X,K,4X,K,6X,K";"PT.NO.","RADIUS IN INCHES","THETA IN D
EG.","FR.ORDER"
710     DISP "INPUT DATA FOR RADIUS(R), THETA(O),FR.ORDER(N)"
720     WAIT 100
730     FOR I=1 TO N3
740     ENTER 701;C(I),X1(I),Y1(I)
750     X6=X1(I)-X5
760     Y6=Y1(I)-Y5
```

```
770     R(I)=M0*SQR(X6^2+Y6^2)
780     O2=ATN(Y6/X6)
790     IF (Y6)=0) AND (X6)=0) THEN O2=O2
800     IF (Y6)=0) AND (X6<0) THEN O2=O2+PI
810     IF (Y6<0) AND (X6<0) THEN O2=O2-PI
820     IF (Y6<0) AND (X6>0) THEN O2=O2
830     A4=O2*180/PI
840     O(I)=A4-A3
850     N(I)=N100+C(I)/2
851     PRINTER IS 0
860     PRINT I,R(I),O(I),N(I)
861     PRINTER IS 16
870     R(I)=R(I)*.0254
880     O(I)=O(I)*PI/180
890     NEXT I
900     INPUT "ITRNS.=?",J
910     REAL L1,L2,L12,L22,I21,I22,I31,I32
920     L12=1-(C/C1)^2
930     L22=1-(C/C2)^2
940     L1=SQR(L12)
950     L2=SQR(L22)
960     FOR L=1 TO J
970     FOR I=1 TO N3
980     S1=SIN(O(I))
990     S2=COS(O(I))
1000    S3=TAN(O(I))
1010    X1=R(I)*S2
1020    Y1=R(I)*L1*S1
1030    X2=X1
1040    Y2=R(I)*L2*S1
1050    F1=ATN(L1*S3)
1060    F2=ATN(L2*S3)
1070    IF (X1)=0) AND (Y1)=0) THEN F1=F1
1080    IF (X1>0) AND (Y1<0) THEN F1=F1
1090    IF (X1<0) AND (Y1>0) THEN F1=3.14159+F1
1100    IF (X1<0) AND (Y1<0) THEN F1=-3.14159+F1
1110    IF (X2)=0) AND (Y2)=0) THEN F2=F2
1120    IF (X2>0) AND (Y2<0) THEN F2=F2
1130    IF (X2<0) AND (Y2>0) THEN F2=3.14159+F2
1140    IF (X2<0) AND (Y2<0) THEN F2=-3.14159+F2
1150    S12=S1^2
1160    S22=S2^2
1170    R01=R(I)*SQR(1-(1-L12)*S12)
1180    R02=R(I)*SQR(1-(1-L22)*S12)
1190    S01=SIN(F1/2)
1200    S02=COS(F1/2)
1210    S03=COS(3*F1/2)
1220    S04=COS(F2/2)
1230    S05=COS(3*F2/2)
1240    S06=COS(F1)
1250    S07=COS(2*F1)
1260    S08=COS(F2)
1270    S09=COS(2*F2)
1280    S010=SIN(3*F1/2)
1290    S011=SIN(F2/2)
1300    S012=SIN(F1)
1310    R21=A0*S02/R01^.5+A1*R01^.5*S02+A2*R01^1.5*S03
1320    R22=A0*S04/R02^.5+A1*R02^.5*S04+A2*R02^1.5*S05
1330    R31=B0+B1*R01*S06+B2*R01^2*S07
1340    R32=B0+B1*R02*S08+B2*R02^2*S09
1350    I21=-A0*S01/R01^.5+A1*R01^.5*S01+A2*R01^1.5*S010
1360    I22=-A0*S011/R02^.5+A1*R02^.5*S011+A2*R02^1.5*SIN(3*F2/2)
1370    I31=B1*R01*S012+B2*R01^2*SIN(2*F1)
1380    I32=B1*R02*SIN(F2)+B2*R02^2*SIN(2*F2)
1390    W=4*L1*L2/(1+L22)
1400    D(I)=(W*R22-(1+L12)*R21)/(W-(1+L22))+((1+L22)*R32-(1+L12)*R31)/(L12-L22)
1410    T(I)=2+L1*(I22-I21)/(W-1-L22)+((1+L22)^2*I32/(2*L2)-2*L1*I31)/(L12-L22)
1420    G(I)=D(I)^2+T(I)^2-(N(I)*F/(2*H))^2
1430    D1=(W*S04/R02^.5-(1+L12)*S02/R01^.5)/(W-1-L22)
1440    D2=(W*S04*R02^.5-(1+L12)*R01^.5*S02)/(W-1-L22)
1450    D3=(W*S05*R02^1.5-(1+L12)*S03*R01^1.5)/(W-1-L22)
1460    D4=-1
1470    D5=((1+L22)*R02*S08-(1+L12)*R01*S06)/(L12-L22)
1480    D6=((1+L22)*R02^2*S09-(1+L12)*R01^2*S07)/(L12-L22)
1490    T1=(S01/R01^.5-S011/R02^.5)*2*L1/(W-1-L22)
1500    T2=2*L1*(S011*R02^.5-S01*R01^.5)/(W-1-L22)
1510    T3=2*L1*(R02^1.5*SIN(1.5*F2)-R01^1.5*S010)/(W-(1+L22))
1520    T4=0
1530    T5=((1+L22)^2*R02*SIN(F2)/(2*L2)-2*L1*R01*S012)/(L12-L22)
1540    T6=((1+L22)^2*R02^2*SIN(2*F2)/(2*L2)-2*L1*R01^2*SIN(2*F1))/(L12-L22)
1550    A(I,1)=2*D(I)*D1+2*T(I)*T1
1560    A(I,2)=2*D(I)*D2+2*T(I)*T2
1570    A(I,3)=2*D(I)*D3+2*T(I)*T3
1580    A(I,4)=2*D(I)*D4+2*T(I)*T4
1590    A(I,5)=2*D(I)*D5+2*T(I)*T5
1600    A(I,6)=2*D(I)*D6+2*T(I)*T6
1610    NEXT I
```

```
1620   MAT U=TRN(A)
1630   MAT P=U*G
1640   MAT Q=U*A
1650   MAT W=INV(Q)
1660   MAT Y=(-1)*W
1670   MAT X=Y*P
1680   A0=A0+X(1)
1690   A1=A1+X(2)
1700   A2=A2+X(3)
1710   B0=B0+X(4)
1720   B1=B1+X(5)
1730   B2=B2+X(6)
1731   IF L>J-4 THEN 1733
1732   GOTO 1740
1733   PRINTER IS 0
1740   PRINT "ITERATION NO.=",L
1750   PRINT "------------"
1760   PRINT "INTERMEDIATE A0 ETC.=",A0,A1,A2,B0,B1,B2
1770   MAT G=ZER(N3)
1780   FOR I1=1 TO N3
1790   N1(I1)=SQR(D(I1)^2+T(I1)^2-G(I1))*2*H/F
1800   N2(I1)=ABS(N(I1)-N1(I1))
1810   NEXT I1
1820   FOR I2=2 TO N3
1830   N2(I2)=N2(I2)+N2(I2-1)
1840   NEXT I2
1850   N60=N2(N3)/N3
1851   PRINT "AVERAGE FR.ORDER ERROR=",N60
1852   PRINTER IS 16
1860   NEXT L
1870   K1=A0*SQR(2*PI)
1871   PRINTER IS 0
1880   PRINT "FINAL VALUES OF THE SIX PARAMETERS ARE:-"
1890   PRINT "----------------------------------------"
1900   PRINT USING "K";" K1="," ",K1,"    ","MPA-SQR(METER)"
1910   PRINT USING "K";" A1="," ",A1,"    ","MPA/SQR(METER)"
1920   PRINT USING "K";" A2="," ",A2,"    ","MPA/M^1.5"
1930   PRINT USING "K";" B0="," ",B0,"    ","MPA"
1940   PRINT USING "K";" B1="," ",B1,"    ","MPA/M"
1950   PRINT USING "K";" B2="," ",B2,"    ","MPA/M^2"
1951   PRINTER IS 16
1960   DISP "IF THE PARAMETERS HAVEN'T CONVERGED DON'T USE THE VALUES"
1970   WAIT 3000
1980   END
```

BIBLIOGRAPHY

Anthony S.R. and Congleton, J., "Crack Branching in Strong Metals," Metals Science, Vol. 2, pp. 158-160, 1968.

Chandar, Ravi K., "An Experimental Investigation into the Mechanics of Dynamic Fracture," Ph.D. Thesis, California Inst. of Tech., pp. 124, 1982.

Clark, A.B.J., and Irwin, G.R., Crack Propagation Behaviors," Exp. Mech. 6, 321-330, 1966.

Congleton, J., "Practical Applications of Crack Branching Measurements," Proc. of Dynamic Crack Propagation (ed. G.C. Sih) Lehigh University; Noordhoff Int. Publishing, 1972.

Craggs, J.W., "On the Propagation of a Crack in an Elastic Brittle Material," J. Metals Phy. Solids, Vol. 8, pp. 67-75, 1960.

Cranz, C. and Schardin, H., Zeits. f. Phys., 56, 147-83, 1929.

Dally, J.W., "Dynamic Photoelastic Studies of Fracture," Experimental Mechanics, Vol. 19, No. 10, -p. 349-361, October 1979.

Dally, J.W. and Riley, W.F., "Experimental Stress Analysis," McGraw-Hill, p. 406, 1978.

Dixon, J.R., "Stress and Strain Distributions around Cracks in Sheet Materials Having Various Work Hardening Characteristics," Intl. Journal of Fracture Mechanics, 1(3), pp. 224-244 (1965).

Doll, W., "Investigations of the Crack Branching Energy," Int. J. of Fracture, 11, 184, 1975.

Gerberich, W., Stress Distribution about a Slowly Growing Crack Determined by the Photoelastic-Coating Technique," Experimental Mechanics, 2(12), pp. 359-365 (1962).

Irwin, G.R., "Constant Speed Semi-Infinite Tensile Crack Opened by a Line Force, P, at a Distance b, from the Leading Edge," Lehigh University Lecture Notes.

Irwin, G.R., "Discussion of Reference 5," Proc. of SESA, 16(1), pp. 93-96 (1958).

Irwin, G.R. et al, "On the Determination of the $\dot{a}$-K Relationship for Birefringent Polymers," Experimental Mechanics, Vol. 19, No. 4, pp. 121-128, April 1979.

Irwin, G.R. et al, "A Photoelastic Characterization of Dynamic Fracture," Univ. of Maryland Report, pp. 87-93, Dec. 1976.

Kalthoff, J.F., "On the Propagation Direction of Bifurcated Cracks," Proc. of "Dynamic Crack Propagation," (ed. G.C. Sih), Lehigh University, Noordhoff Int. Publishing, pp. 449-458, 1972.

Kirchner, H.P., "The Strain Intensity Criterion for Crack Branching in Ceramics," Eng. Frac. Mech., Vol. 10, pp. 283-288, 1978.

Kobayashi, A.S. et al, "Crack Branching in Homalite 100 Sheets," Engg. Fracture Mechanics, Vol. 6, pp. 81-92, 1974.

Kobayashi, T. and Dally, J.W., "A System of Modified Epoxies for Dynamic Photoelastic Studies of Fracture," Experimental Mechanics, 17(10), pp. 367-374 (1977).

Post, D., "Photoelastic Stress Analysis for an Edge Crack in a Tensile Field," Proc. of SESA, 12(1), pp. 99-116 (1954).

Ramulu, M. et al, "Dynamic Crack Branching - A Photoelastic Evaluation," ONR Technical Report No. UWA/DME/TR-82/43.

Rossmanith, H.P., "Crack Branching in Brittle Materials - Part I," University of Maryland Report 1977-80.

Rossmanith, H.P. and Irwin, G.R., "Analysis of Dynamic Isochromatic Crack Tip Stress Patterns," University of Maryland Report.

Rossmanith, H.P. and Shukla, A., "Dynamic Photoelastic Investigation of Interaction of Stress Waves with Running Cracks," Exp. Mech., pp. 415-422, Nov. 1981.

Sanford, R.J. and Dally, J.W., "A General Method for Determining Mixed Mode Stress Intensity Factors from Isochromatic Fringe Patterns," J. of Engr. Fract. Mech., 11, 621-633 (1979).

Sanford, R.J. et al, "A Photoelastic Study of the Influence of Non-Singular Stresses in Fracture Test Specimens," University of Maryland Report, p. 1, Aug. 1981.

Schroedl, M.A., McGowen, J.J. and Smith, C.W., "Assessment of Factors Influencing Data Obtained by the Photoelastic Stress Freezing Technique for Stress Fields near Crack Tips," Journal of Engg. Fract. Mechanics, 4(4), pp. 801-809 (1972).

Shukla, A., "Crack Propagation in Ring Type Fracture Specimens," M.S. Thesis, University of Maryland, p. 50, 1979.

Wells, A. and Post, D., "The Dynamic Stress Distribution Surrounding a Running Crack - A Photoelastic Analysis," Proc. of SESA, 16(1), pp. 69-92 (1958).

Yoffe, E.H., "The Moving Griffith Crack," Philosophical Magazine, Series 7, 42, 739 (1951).